

Dalton Transactions

Accepted Manuscript



This is an *Accepted Manuscript*, which has been through the Royal Society of Chemistry peer review process and has been accepted for publication.

Accepted Manuscripts are published online shortly after acceptance, before technical editing, formatting and proof reading. Using this free service, authors can make their results available to the community, in citable form, before we publish the edited article. We will replace this *Accepted Manuscript* with the edited and formatted *Advance Article* as soon as it is available.

You can find more information about *Accepted Manuscripts* in the [Information for Authors](#).

Please note that technical editing may introduce minor changes to the text and/or graphics, which may alter content. The journal's standard [Terms & Conditions](#) and the [Ethical guidelines](#) still apply. In no event shall the Royal Society of Chemistry be held responsible for any errors or omissions in this *Accepted Manuscript* or any consequences arising from the use of any information it contains.

TOPOTACTIC CONDENSATION OF LAYER SILICATES WITH FERRIERITE-TYPE LAYERS FORMING POROUS TECTOSILICATES

B. Marler,^{*a} Y. Wang,^b J. Song,^c and H. Gies^a

^a Dept. of Geology, Mineralogy and Geophysics, Ruhr University Bochum, D-44780 Bochum, Germany, E-mail: bernd.marler@rub.de; Tel: (+49) 234-32-23514

^b College of Chemistry and Molecular Engineering, Peking University, Beijing 100871, China

^c Beijing University of Chemical Technology, State Key Lab of Chemical Resource Engineering, Beijing 100029, China.

ABSTRACT

Five different Hydrous Layer Silicates (HLSs) containing fer layers (Ferrierite-type layers) were obtained by hydrothermal syntheses from mixtures of silicic acid, water and tetraalkylammonium/tetraalkylphosphonium hydroxides. The organic cations had been added as structure directing agents (SDA). A characteristic feature of the structures is the presence of strong to medium strong hydrogen bonds between the terminal silanol/siloxy groups of neighbouring layers. The five layered silicates differ chemically only with respect to the organic cations. Structurally, they differ with respect to the arrangement of the fer layers relative to each other which is distinct for every SDA-fer-layer system. RUB-20 (containing tetramethylammonium) and RUB-40 (tetramethylphosphonium) are monoclinic with stacking sequence AAA and shift vectors between successive layers $1a_0+0b_0+0.19c_0$ and $1a_0+0b_0+0.24c_0$, respectively. RUB-36 (diethyldimethylammonium), RUB-38 (methyltriethylammonium) and RUB-48 (trimethylisopropylammonium) are orthorhombic with stacking sequence ABAB and shift vectors $0.5a_0+0b_0\pm 0.36c_0$, $0.5a_0+0b_0+0.5c_0$ and $0.5a_0+0b_0\pm 0.39c_0$, respectively.

Unprecedented among the HLSs, two monoclinic materials are made up by fer layers which possess a significant amount of ordered defects within the layer. The ordered defects involve one particular Si-O-Si bridge which is to a fraction of ca. 50% hydrolyzed to form nests of two $\equiv\text{Si-OH}$ groups.

When heated to 500-600°C in air the HLSs condense to form framework silicates. Although all layered precursors were moderately to well ordered, the resulting framework structures were of quite different crystallinity. The orthorhombic materials RUB-36, -38 and -48, general formula $\text{SDA}_4\text{Si}_{36}\text{O}_{72}(\text{OH})_4$, which possess very strong hydrogen bonds ($d[\text{O}\dots\text{O}] \approx 2.4 \text{ \AA}$) transform into a fairly or well ordered **CDO**-type silica zeolite RUB-37. The monoclinic materials RUB-20 and -40, general formula $\text{SDA}_2\text{Si}_{18}\text{O}_{36}(\text{OH})_2\text{OH}$, possessing medium strong hydrogen bonds ($d[\text{O}\dots\text{O}] \approx 2.65 \text{ \AA}$) are transformed into poorly ordered framework silicates. Some rules of thumb can be established concerning the successful zeolite synthesis via a topotactic condensation of layered precursors. Favourably, the precursor (i) possesses already a well ordered structure without defects, (ii) contains strong **inter-layer** hydrogen bonds and does not contain strong **intra-layer** hydrogen bonds and (iii) contains a suitable cation. The nature of the organic cation (size, geometry, flexibility, thermal stability) plays the key role for the formation of a microporous tectosilicate with well ordered structure. RUB-36 which meets these criteria yields a well ordered condensation product (RUB-37).

Introduction

Layer silicates are used for many different purposes such as binder and supports in catalysts application or filler in paper manufacture and are very interesting materials in their as made form. In addition, these silicates can be modified in many ways e.g. by ion exchange, intercalation, and swelling. During the past ten years layered silicates were also used as precursors for the preparation of new micro- and mesoporous materials by the techniques of pillaring,^{e.g. 1, 2}, delamination^{e.g. 3-5a} and topotactic condensation.^{e.g. 6, 7, 8}

The layered materials discussed here belong to the group of Hydrous Layer Silicates (**HLSs**) which contain cations of low charge density between the layers (unlike for example micas or clays). Such cations are predominantly organic cations but also hydrated inorganic cations like sodium-water complexes $[\text{Na}(\text{H}_2\text{O})_6]^+$ can be present. These HLSs are typically prepared via classical hydrothermal synthesis techniques using a particular structure directing agent (SDA). The SDA is usually an amine or an ammonium compound, in some cases phosphonium cations or hydrated alkali metal ions like $[\text{Na}(\text{H}_2\text{O})_6]^+$ ^{e.g. 9} or a combination of inorganic and organic SDAs are used.^{e.g. 10}

In many cases, the topology of the layer of the HLS silicate is identical to a layer-like building unit (LLBU) of a known zeolite framework.⁸ In particular, Ferrierite-type silicate layers (fer layers) seem to form easily under hydrothermal conditions from aqueous solutions of silicic acid and one of several specific organic SDAs. So far, about 12 different SDAs are reported in the literature which have successfully been used to form layered silicates with fer layers (Table 1).^{7, 10-18}

The topotactic condensation of layer silicates into microporous framework materials has so far been described rarely. The first successful example was reported for zeolites with the MWW framework type. These materials were described 10 to 20 years ago.⁶ According to the open literature, there are now several layer silicates with different layer topologies which were successfully converted into zeolites (microporous framework silicates) by topotactic condensation of the layers: AST (type material: β -Helix-Layered-Silicate¹⁹), CAS (type material: EU-20, EU-20b^{20, 20a}), CDO (type material: CDS-1¹⁰), FER (type material: siliceous Ferrierite⁷) MTF (type material: HPM-2²¹), MWW (type material: MCM-22⁶), NSI (type material: NU-6(2)²²), RRO (type material: RUB-41²³), RWR (type material: RUB-24²⁴) SOD (type material: guest-free Silica Sodalite^{25,25a}) For the “zeolite framework type codes” and the crystal structures of the corresponding materials see Baerlocher et al..²⁶ In this way four new zeolite framework types were observed which have not been obtained by direct hydrothermal synthesis so far (CDO, NSI, RRO, RWR).

This paper describes the preparation and the crystal structure analyses of several silicates containing fer layers. In a series of synthesis experiments using derivatives of the tetramethylammonium cation we investigated the influence of the geometry of the SDA on the structure of the layer silicate being formed and on the consequences on a subsequent condensation reaction which sometimes results in the formation of zeolitic material.

The fer layer as a building block in silicate structures

The fer layer (Fig. 1) is a non-porous layer consisting only of 5-rings of [SiO₄]-tetrahedra. The 5-rings form complex composite building units (CBUs) of the fer-type²⁶ which, in turn, compose the complete fer layer by sharing common edges. The layer has a thickness of about 9.5 Å (not counting the v.d.Waals radii of the layer terminating oxygen atoms) which is equivalent to 9 atomic layers. Within the plane of the layer a 2-dimensional unit cell exists with lattice parameters of $b \approx 14.0$ Å and $c \approx 7.5$ Å. Throughout this paper it will be always referred to the setting of the unit cell as shown in Fig. 1 with intra-layer dimensions of 14.0 and 7.5 Å and the a-axis being orientated perpendicular to the plane of the layer (\approx stacking direction). There are only few terminal oxygen atoms: 4 out of 18 SiO₄ tetrahedra (per unit cell) are only 3-connected to other tetrahedra. Moreover, these terminal silanol (\equiv Si-OH) or siloxy (\equiv Si-O⁻) groups have a rather large distance of at least 5.7 Å between each other. It is, therefore, unlikely that an intra-layer condensation of these groups would occur if a layered material containing fer layers is heated. This structural feature makes the fer layer a very interesting building block for a transformation into a microporous framework material.

By heating layer silicates in air at temperatures between 400 - 600°C they can be transformed into porous tectosilicates. If fer layers are interconnected by topotactic condensation two simplest ordered framework topologies can be generated: the zeolite framework types FER (Ferrierite) and CDO (zeolite CDS-1) (Fig. 2). In Ferrierite, neighbouring layer-like building units (LLBUs) are shifted by a vector of $1/2 b + 1/2 c$ generating an orthorhombic ABAB-stacking, with lattice parameters of $a = 19.0$ Å, $b = 14.2$ Å and $c = 7.5$ Å (highest possible space group symmetry: Immm). Ferrierite has a 2-dimensional pore system of 8- and 10-ring channels running along [010] and [001], respectively. In the case of the CDO-type framework neighbouring LLBUs are shifted by a vector of $0 b + 1/2 c$ forming a different orthorhombic lattice with ABAB-stacking of the LLBUs and lattice parameters of $a = 18.7$ Å, $b = 14.2$ Å and $c = 7.5$ Å (highest possible space group symmetry: Bbmm, No. 63). The pore system of the CDO-type consists of intersecting 8-ring channels extending along the [010] and [001] direction.

Experimental

Synthesis

In our study, six different tetraalkylammonium ions and one tetraalkylphosphonium ion were used as structure directing agents to investigate the influence of the geometry of the organic species on the structure of the silicate being formed during the synthesis. In addition, the structure of the material obtained by a subsequent topotactic condensation was also investigated. The syntheses were performed in a very simple system comprising only the structure directing agent (SDA) as hydroxides, a silica source and water. There is one exception: in the case of methyltriethylammonium the fluoride was used. The resulting product, named RUB-38, however, did not contain any fluorine. The synthesis conditions are given in Table 2. The SDAs are listed according to their carbon to nitrogen ratio. The following cations were used as SDAs: tetramethylammonium, tetramethylphosphonium, trimethylisopropylammonium, diethyldimethylammonium, methyltriethylammonium, dimethyldiisopropylammonium and dimethyldi-n-propylammonium.

The reaction mixtures were prepared by combining appropriate amounts of SiO₂ and the aqueous SDAOH solution. The mixtures were homogenized by stirring. Then the water content was adjusted by either removing excess water by evaporation at 70°C in an oven or some water was added. The homogenized mixtures were then transferred into a Teflon-lined stainless steel autoclave and heated at 150° C to 170°C for 2 to 4 weeks. After crystallization the autoclaves were quenched in cold water. The solid product was recovered by filtration, washed with distilled water and then dried overnight at 60°C.

The condensation products were obtained by heating the as-synthesized layer silicates in air from room temperature up to 500°C - 600 °C with a heating rate of 2°/min. The samples were held at that temperature for several hours until the white colour of the sample indicated that the organic material was completely removed.

General Characterization

Scanning electron microscopy (SEM) investigations to study the morphology of the crystals and the homogeneity of the samples were performed using a LEO-1530 Gemini electron microscope.

Thermal properties of the as-synthesized materials were investigated by simultaneous DTA/TG measurements using a Bähr STA-503 thermal analyzer. The samples were heated in synthetic air from 40 to 1000°C with a heating rate of 10°C/min.

Solid state MAS NMR spectra were recorded at room temperature with a Bruker ASX-400 spectrometer using standard Bruker MAS probes. In order to average the chemical shift anisotropy, samples were spun about the magic angle. Recording conditions are listed in Table 3. In all cases TMS was used as a chemical shift standard. Concerning the ^{29}Si NMR spectra mainly hpdec MAS measurements were performed (with one exception) to calculate realistic $Q^3 : Q^4$ ratios from the signal intensities. Only in the case of RUB-38 a CP MAS recording was used to gain detailed information on the symmetry of the material.

Diffraction experiments

The crystals of the layer silicates and of the condensation products were too small and had a too low scattering power to analyze their structure by conventional single crystal work. Therefore, XRD data were recorded from powder samples in glass capillaries ($\varnothing = 0.3 \text{ mm}$), on a Siemens D5000 powder diffractometer in Debye-Scherrer geometry using $\text{CuK}\alpha_1$ radiation ($\lambda = 1.5406 \text{ \AA}$). The diffractometer was equipped with a curved germanium (111) primary monochromator and a linear position-sensitive detector ($6^\circ 2\theta$).

Reflections were indexed using the program TREOR²⁷ as implemented in WINPLOTR.²⁸ High resolution synchrotron powder diffraction data from a RUB-36 sample sealed in a capillary were recorded at beam line B2 at HASYLAB, Hamburg. A Ge (111) double crystal monochromator was used to obtain a monochromatic beam with $\lambda = 1.1314 \text{ \AA}$. Intensity data were recorded at ambient conditions in Debye-Scherrer-geometry in the 2θ range $5.5 - 50.0^\circ$ with steps of 0.003° .

Structure analysis

The materials were either identified by comparing their powder XRD patterns with the patterns of known compounds (e.g. zeolites Nonasil (NON), CDO-type zeolite (CDO), Dodecasil 3C (MTN)²⁹ and layer silicates ERS-12,¹³ MCM-47¹¹) or at least the silicate layer type of the materials synthesized was recognized after indexing the powder XRD patterns. Lattice parameters of $b_0 \approx 7.4 \text{ \AA}$ and $c_0 \approx 14.0 \text{ \AA}$ with an angle of 90° between the b and c axis are likely to be attributed to fer layers being present as building blocs in the material.

In spite of some differences concerning the symmetry and the occluded organic cation which exist between the new layered RUB phases and the phases known from the literature, it was possible to build approximate structure models that served as starting models for the structure refinements. These models were generated based on the geometries of known structures but taking

into account the particular lattice parameters and space group symmetry of the newly synthesized materials.

For the Rietveld refinements of the powder data sets the FullProf 2K program system³⁰ was used with atomic scattering factors taken as implemented in the program. Details of the structure analyses and crystallographic parameters of the five layered materials RUB-20 (+ RUB-20b for confirmation), RUB-36, RUB-38, RUB-40 and RUB-48, and the framework material RUB-37, are listed in Table 4. In all cases the refinement had to be performed using anisotropic broadening of the peak halfwidths. The broadening is due to a slight disorder of the layer stacking and to a much lesser extend to the specific morphology (thin platelets). All 0kl reflexions representing the atomic arrangement within the layer are sharp, all h00 reflexions representing the interlayer distances are moderately sharp, but all hkl reflexions with $h, k, l \neq 0$ are broadened. These reflexions include also information on the orientation of layers relative to each other which is not perfect because of weak bonding interactions between neighbouring layers.

Results

Layer silicates

Synthesis

The hydrothermal syntheses using the cations tetramethylammonium, tetramethylphosphonium, trimethylisopropylammonium, diethyldimethylammonium and methyltriethylammonium with C : N ratios of 4 to 7 led to the formation of five different layer silicates (Tab. 2). These silicates are all made up by *fer* silicate layers intercalated by the particular cation which was added as the SDA during synthesis.

At synthesis temperatures of 175°C and higher the same SDAs led predominantly to the formation of microporous framework silicates. At temperatures $\geq 175^\circ\text{C}$, materials with zeolite framework types **NON** (Nonasil) or **MTN** (Dodecasil 3C) - both containing cage-like voids - are formed. This result might be explained by a partial decomposition of the SDA forming amine molecules via possible reactions $\text{NR}_4^+ + \text{OH}^- \rightarrow \text{R}_3\text{N} + \text{R-OH}$, or $\text{NR}_4^+ + \text{OH}^- \rightarrow \text{R}_3\text{N} + \text{H}_2\text{O} + \text{R=}$ (with R= being the corresponding alkene). The amine then can act as the SDA for the crystallization of porous materials with a neutral SiO_2 framework structure. SDAs with a C : N ratio = 8 gave microporous framework silicates in this synthesis series (**DOH**, **MFI**, **NON**), even at the relatively low synthesis temperature of 150°C. The very low charge densities of these big cations are probably the reason that they favour the crystallization of framework silicates with some random Si-O⁻ defects compensating the charge of the SDA and do not form silicate layers having numerous negatively charged siloxane groups.

The HLSs were obtained below 175 °C. The optimum conditions for the different phases are summarized in Table 2. The compilation is in agreement with the observation made for the synthesis of porous silicates: in systems where several phases are formed, the framework silicates with high framework density crystallize at higher synthesis temperatures.³¹

General Characterisation

All layer silicates crystallize as thin colorless crystals with a plate-like morphology (Fig. 3, top). The diameter of the crystals is typically in the range of 2 to 10 µm with a thickness of about 0.1 µm.

X-ray analysis

The X-ray powder diagrams of all six layer silicates are presented in Figure 4. Depending on the type of material the XRD diagrams of these silicates show sharp to fairly sharp reflexions which indicate that the samples are well or moderately crystalline. Two of the five materials, RUB-20, RUB-40, are monoclinic while the remaining ones, RUB-36, RUB-38 and RUB-48 have an orthorhombic lattice symmetry (see also Table 4.) From the comparison of the powder diagrams, RUB-20 is regarded to be nearly identical to ERS-12.¹³ RUB-40 is similar to PLS-1¹⁰ and ERS-12¹³ with respect to the structural arrangement of the silicate layers but possesses another organic cation intercalated between the layers. RUB-38 is structurally related to MCM-47¹¹ and MCM-65¹² considering the arrangement of the silicate layers in the structure but also possesses a different organic cation. RUB-36 and RUB-48, finally, are closely related to PLS-4^{15a} and UZM-13.¹⁶

NMR spectroscopy

The solid-state ²⁹Si NMR spectra of the layer silicates showed two groups of signals around – 102 ppm and -112 ppm, respectively. Figure 5 presents the spectra of RUB-20 and RUB-36 as representatives of the monoclinic and orthorhombic materials, respectively. Chemical shift values between -105 and -116 ppm are typical for 4-connected SiO₄-units (or Q⁴-units), Si(-O-Si)₄-groups, while the signals between -96 and -105 ppm represent the terminal 3-connected SiO₄-units (or Q³-units) of the silicate layer which are of the type Si(-O-Si)₃(-OH) or Si(-O-Si)₃(-O). Table 5 lists the observed signals with chemical shift values and relative intensities for all investigated materials.

The idealized fer layer has a Q³ : Q⁴ intensity ratio of 1 : 3.5 since there are four terminal silanol groups and fourteen 4-connected SiO₂ units per 2-dimensional unit cell of the layer. The three orthorhombic materials show signals with Q³ : Q⁴ intensity ratios of 1 : 3.0 to 1 : 3.9. This is close to the expected value. All monoclinic materials possess a considerably smaller Q³ : Q⁴ ratio indicating that there are additional defects in the silicate layers leading to an increased number of

silanol groups (Q^3 -units). This phenomenon will be discussed in detail in the structure analysis section.

The ^{13}C CP NMR spectra (Fig. S1 of the Supplement) of the six layered silicates present one to three sharp signals in the range between 8 ppm and 70 ppm. The respective values are listed in Table S1 (Supplement) together with the expected shift values as estimated from the molecular structure of cations. In all cases, the SDA used for the synthesis was occluded as organic cation compensating the layer charge.

Besides some weaker signals, the proton MAS NMR spectra of the six layered silicates show one or two strong resonance lines depending on the particular type of organic cation included in the structure of the given silicate: A signal at ca. 1.5 ppm is assigned to the methylene groups of the organic cation while a signal at ca. 3.5 ppm corresponds to the protons of the methyl group of the cation. The latter resonance signal also includes the protons of the water molecules if present in the structure. Figure 6 presents the spectra of RUB-20 and RUB-36 as representatives of the monoclinic and orthorhombic materials, respectively.

In addition to these strong signals there are weaker signals corresponding to the protons of the silanol groups (Tab. 6). The six spectra may best be divided in two groups: the spectra of the orthorhombic materials RUB-36, RUB-38 and RUB-48, and the monoclinic materials RUB-20, RUB-20b and RUB-40.

The spectra of the orthorhombic silicates present only one additional, fairly sharp signal at ca. 16.2 ppm. A shift value of 16.2 ppm corresponds to a strong hydrogen bond with an O...O distance of about 2.4 Å or an O...H bond length of ca. 1.5 Å.^{32, 33} Such low field chemical shift values have been observed for several Hydrous Layer Silicates (HLSs) which possess short hydrogen bonds between neighbouring silanol groups, e.g. RUB-18 (a sodium silicate) 15.9 ppm,³⁴ MCM-47 (containing fer layers) 16.6 ppm¹¹ and RUB-39 (a layer silicate with Heulandite-type layers) 16.4 ppm.³⁵ These strong hydrogen bonds were observed between neighbouring layers (**inter-layer**) as well as between neighbouring siloxane units within the silicate layer (**intra-layer**).

The sharpness of the signal moreover indicates that the hydrogen bonds are isolated from each other and are not subject to exchange reactions.

For the monoclinic layer silicates the ^1H MAS NMR spectra exhibit a more complex pattern: In addition to the strong signal of the methyl groups at ca. 3.5 ppm for tetramethylammonium and at 2.1 ppm for tetramethylphosphonium, three weak signals are visible in each case with chemical shift values of 5.5 to 13.6 ppm. One of these signals can be assigned to hydrogen bonds between

neighbouring layers, the two other signals correspond probably to protons of acidic silanol groups related to defects of the layer (refer to Tab. 6 and see also the structural studies, below).

Thermal analysis

The general features of the DTA curves are similar for all layer silicates investigated in this study. For all samples containing an ammonium compound as guest species (RUB-20, 20b, -36, -38, -48) there is an endothermic signal around 350°C and an exothermic signal at ca. 400°C. The exact temperatures of the reactions, however, differ depending on the particular composition (Tab. 7). The main weight loss occurs between 300 and 430°C. The experimentally observed total weight loss is, except for RUB-40, in all cases close to the expected value calculated from the idealized composition of the material. Only the phosphonium ion included in the structure of RUB-40 does not leave the material completely. It might partly be oxidized to form a phosphate; the gray colour of the calcined sample, on the other hand, indicated that there is still some carbon present which could not be removed. The weight loss of RUB-40 is therefore much lower than the calculated sum of masses of the organic cation and water generated by the condensation of silanol groups (Tab. 7).

As an example the TG and DTA curves of RUB-36 are given (Fig. 7). The TG curve shows a first small weight loss of 1% at about 90°C which is assigned to the loss of physically adsorbed water. In accordance, the DTA curve shows a first very small endothermic signal also at 90°C. A second endothermic signal with a minimum at 373°C is interpreted as a decomposition of the cation plus partial desorption of organic material and/or the beginning of the silanol condensation reaction. This event is immediately followed by two exothermic signals (413 and 439°C) indicating the burn off of the (remaining) organic species. The temperature and the exothermic character of the signals at ca. 420°C is typical for the combustion of organic material. After the corresponding steep descent of the TG curve a much slower release of the organic remains is visible in the temperature range between ca. 430°C and 750°C. This is an indication that the silicate layers are condensed to a framework silicate with much smaller pore openings which hamper the further oxidation and expulsion of the organic matter.

The total weight loss of ca. 18.6% occurring between 300 and 750°C accounts for the expulsion of the diethyldimethylammonium cations and the water generated by the condensation of the silanol groups. A complete condensation of all silanol groups of the layer leads to the formation of 4 water molecules per unit cell: $[\text{H}_4\text{Si}_{36}\text{O}_{76}]^{4-} * 4 \text{HR}^+ \Rightarrow \text{Si}_{36}\text{O}_{72} + 4 \text{H}_2\text{O} + 4 \text{R}$.

The thermal analyses indicate that the condensation of the silanol groups and the burn off of the organic material happens at about the same temperature.

All layered silicates investigated in this study turn black at ca. 400°C. Only after heating the materials up to ca. 800°C the samples become colorless again indicating that all organic material has finally left the structure.

Structure analysis

General Considerations

A detailed structure analysis is essential to elucidate structure-property relations and to reveal especially those structural features which might have an influence on the topotactic condensation process.

The structures of RUB-20, RUB-40 and RUB-38 were determined by comparing their XRD patterns with those of other layer silicates. It was obvious that RUB-20 and RUB-40 are closely related to ESR-12 and PLS-1 while RUB-38 is related to MCM-47 and MCM-65. In the case of RUB-36 and RUB-48 no directly corresponding material was found in the literature at that time. The structures were, therefore, solved by model building (see below). Later it was recognized that UZM-13¹⁶ is chemically and structurally nearly identical to RUB-36.

After successfully indexing, the possible space group symmetries of the materials were determined by an analysis of the systematic extinctions in their powder XRD-pattern. For each of the six materials the possible space group symmetries could be limited to two: $P2_1/m$ (No.11) and $P2_1$ (No. 6) in the case of RUB-20, RUB-20b and RUB-40; $Bbmm$ (No. 63) and $Bb21m$ (No. 36) for RUB-38; and $Pnma$ (No.62) and $Pn2_1a$ (No. 33) for RUB-36 and RUB-48.

In a first step of the Rietveld refinements the profile parameters (lattice parameters, zero point, halfwidth parameters, asymmetry parameters) were refined using the LeBail-fit technique. The powder patterns of all structures showed anisotropic peak broadening which is typical for HLSs. In order to account for the anisotropic halfwidth additional parameters had to be included into the profile fit.

Subsequently the structural parameters of the silicate layer were refined. Since the starting models did not include meaningful coordinates for the atoms of the organic cations, these constituents were located from difference Fourier maps after refining the Si and O positions of the silicate layer. Soft distance restraints were used in the refinement for $d(\text{Si-O}) = 1.62(1) \text{ \AA}$, $d(\text{Si...Si}) = 3.10(3) \text{ \AA}$, $d(\text{O...O}) = 2.62(2) \text{ \AA}$, $d(\text{N-C}) = 1.50(1) \text{ \AA}$ $d(\text{P-C}) = 1.85(1) \text{ \AA}$. Displacement parameters $B(\text{iso})$ for crystal chemically similar atoms like all Si atoms or all oxygen atoms of the silicate layer were constrained to be equal. The details of data collection and the results of the structure refinement are summarized in Table 4.

The hydrogen atoms could not be located. To account for the scattering power of the hydrogen atoms the occupancy factor of the carbon atoms representing the methyl or methylene groups was

increased by a factor of 1.5 or 1.333, respectively. Similarly, the occupancy factor of the oxygen atom representing a water molecule was increased by a factor of 1.25. This procedure was chosen because the displacement parameters of the carbon and oxygen atoms are quite large and the diffuse electron density at the position of the carbon and oxygen atoms includes also the electrons of the hydrogen atoms. Inclusion of the electrons in the refinement leads to a significant improvement of the residuals.

For the further discussion of the crystal structures, it is meaningful to subdivide the analyses into two groups and to discuss the orthorhombic and the monoclinic materials separately:

The structures of the orthorhombic materials

An initial structure model for the Rietveld refinement of the RUB-38 structure was derived from the structure of MCM-47.¹¹

Attempts to solve the remaining orthorhombic structures of RUB-36 and RUB-48 by Direct Methods from the powder diffraction data failed. The lattice parameters of both phases are approx. $a_0 = 22.25 \text{ \AA}$, $b_0 = 14.01 \text{ \AA}$, $c_0 = 7.39 \text{ \AA}$, and indicate that these materials are also layer silicates with fer type layers.

To construct a first rough structure model of RUB-36 the framework structure of ferrierite was formally divided into identical fer layers. To do so, the Si-O-Si bridges between the layer-like building units (LLBU) of the framework were cut into -Si-OH and HO-Si- groups. The distance between neighbouring silicate layers were then adjusted to the given lattice parameter a_0 of RUB-36. Some carbon atoms applied with a very high displacement parameter were inserted at random into the space between the layers to represent the organic cation. The fer layers were finally shifted relative to each other along the b and c direction for various values. The resulting atomic coordinates were used to calculate XRD patterns which were compared to the experimental pattern of RUB-36 until the simulated and experimental diffraction patterns were very similar. The best model served as the starting model for the structure refinement. Later, the structure model of RUB-48 could easily be obtained from the structure of RUB-36 since the two structures differ only slightly.

As an example of the orthorhombic materials the structure of **RUB-36** is discussed in more detail:

According to structure analysis, TG and NMR spectra, the unit cell content of RUB-36 is $[\text{N}(\text{CH}_3)_2(\text{CH}_2\text{CH}_3)_2]_4[\text{Si}_{36}\text{O}_{72}(\text{OH})_4]$. A reasonable geometry of the diethyldimethylammonium cations (DEDMA cations) is only obtained in space group $\text{Pn}2_1\text{a}$, however, by using geometrical constraints. The refinement results in meaningful distances between organic cation and silicate

layer as well as between the cations (refined without the application of restraints). Figure 8 shows a plot of the experimental and calculated diffraction patterns after Rietveld analysis of RUB-36.

Two fer layers are present per unit cell which are stacked in an ABAB stacking sequence along the *a* axis with an interlayer distance of 11.1 Å. The shift vector between successive layers is: $0.5 \mathbf{a}_0 + 0 \mathbf{b}_0 \pm 0.36 \mathbf{c}_0$. The fer layers show the typical structural features as described in section 2. In RUB-36 each layer is terminated by two silanol groups (Si-OH) and two siloxy groups (Si-O⁻) per unit cell. Figure 9 displays the structures of RUB-36 in two projections. As is shown in the *a*-*c* projection at left hand side, the stacking of layers occurs with an alternative shift to positive and negative values along the *c*-axis relative to the neighbouring layer. With respect to the *b* axis there is no layer shift as shown in the *a*-*b* projection at right hand side.

There are nine symmetrically independent Si atoms and 19 independent oxygen atoms in the structure. Atomic coordinates, displacement parameters, occupancy factors as obtained from the Rietveld refinement as well as bond lengths, bond angles and distances of RUB-36 are provided as Supplementary Info (cif file).

Intercalated between the fer layers there are four DEDMA cations per unit cell. No water was detected in the inter-layer region. Figure 10 depicts a section of the structure highlighting the hydrogen bonds and the orientation of the diethyldimethylammonium cations inside the „channel-like“ voids which are generated by neighbouring silicate layers and hydrogen bonds.

The organic cations are in v.d.Waals contact with each other forming a chain which extends along the *c*-axis. There are no contacts in *b*-direction. In addition, there are v.d.Waals contacts between the methyl groups of the cation and oxygen atoms of the silicate layer.

The RUB-36 structure possesses only isolated hydrogen bonds between the silanol or siloxy groups of neighbouring layers. As expected due to the given topology of the fer layer there are no intra-layer hydrogen bonds. The distance between the two oxygen atoms involved in the bonding (O11 and O12) is 2.32(6) Å and corresponds to a very strong hydrogen bond. This value fits very well to the fairly sharp signal at a chemical shift value of 16.2 ppm as recorded in the ¹H MAS NMR spectrum.

The strong hydrogen bonds together with relatively weak ionic interactions between the large organic cation and the negatively charged silicate layer are important for the stability and the regular stacking registry of the layered structure.

The structure of **RUB-48** is very similar to that of RUB-36. The structure directing effect of the trimethylisopropylammonium cation which is included in the structure of RUB-48 forms a nearly

identical arrangement of fer layers as observed for RUB-36 (containing DEDMA cations). Crystal structure data including interatomic distances and bond angles are provided as Supplementary Info (cif file).

The shift vector between successive layers, $0.5 a_0 + 0 b_0 \pm 0.39 c_0$, and the inter-layer distance along the *a*-axis, $d_{L-L} = 11.1 \text{ \AA}$, are very similar to the values of RUB-36. Also in the case of RUB-48 strong inter-layer hydrogen bonds exist between terminal silanol/siloxy groups with O...O-distances of $2.40(11) \text{ \AA}$.

The use of methyltriethylammonium hydroxide as the SDA led to a new layer silicate named **RUB-38** which also contains fer layers. Its layer arrangement is similar to that of MCM-47 which was synthesized in the presence of tetramethylen-bis(N- methyl)-pyrrolidine.¹¹ RUB-38 has the same layer stacking sequence of ABAB as RUB-36, RUB-38, however, possesses a different shift vector between neighbouring layers: $0.5 a_0 + 0 b_0 + 0.5 c_0$. This type of shift leads to a B-centered lattice and generates a higher symmetry (space group Bbmm) in comparison with RUB-36 (Pn2₁a). Figure 11 shows the structure of RUB-38 including the methyltriethylammonium cations in two projections. In spite of the different shift vectors RUB-38 and RUB-36 possess inter-layer hydrogen bridges of very similar O...O distances: $2.37(2) \text{ \AA}$ and $2.35(6) \text{ \AA}$, respectively. The organic cation is disordered, the refined carbon sites do not reflect the true geometry of the molecule. The methyl groups of the cation are in v.d.Waals-contact with bridging and terminal oxygen atoms of the silicate layer. Crystal structure data including interatomic distances and bond angles are provided as Supplementary Info (cif file, refinement in spacegroup Cmcm (standard setting)).

The structure was refined assuming centrosymmetric symmetry, a reduction of the symmetry (acentric alternative space group Bb2₁m) did not improve the refinement.

The structures of the monoclinic materials

The structures of three different materials were refined: RUB-20 containing tetramethylammonium cations as SDA in the inter-layer space, RUB-40 containing tetramethylphosphonium cations and, additionally for comparison and confirmation, Rub-20b, which also contains the tetramethylammonium cation but was synthesized under different conditions than RUB-20.

All three structures are very similar. RUB-20b and RUB-20 possess nearly identical monoclinic unit cells concerning dimensions and composition (se Tab. 4). The structure of RUB-20b was only analysed to confirm the surprising result of the structure analysis (see below). RUB-40 containing tetramethylphosphonium cations is structurally also closely related to RUB-20 with only minor differences with respect to interlayer distance (d_{L-L}) and shift vector between neighbouring layers

(see Table 8). The refinements will be discussed in the following assuming that the centrosymmetric space group $P2_1/m$ is valid for all three materials (and not in the acentric space group $P2_1$). A more detailed description of the structure analysis of RUB-20 is presented by Marler and Gies.³⁶

An initial structure model for the Rietveld refinements of the monoclinic materials was derived from the structure of ERS-12.¹³ Although the refinements confirmed the correctness of the model concerning the layer topology, the refined structures deviated from the expected structure in one particular detail: During the course of the refinement it became obvious that the position of Si5 which is part of the Q^4 -connected Si in the silicate layer did not refine to the expected distances and angles (refer to Figure 12, top, for the designation of atoms). Although restraints with a moderate weight were applied to all Si-O bonds [$d_{Si-O} = 1.62 (\pm 0.01) \text{ \AA}$], the Si5-O12 distance refined to ca. 2.0 \AA while all other Si-O distances varied in a range of 1.52 to 1.66 \AA - close to the typical Si-O bond length. If Si5 is forced a site yielding a typical bonding distance to O12 ($d_{Si5-O12} = 1.62 \text{ \AA}$) by very strict geometric restraints the R-values increased significantly. Moreover, difference Fourier maps showed an electron density maximum close to Si5 within a distance of ca. 1.9 \AA .

Moreover, if the occupancy factor of O12 was refined it decreased from 100% to a value of 51% (RUB-20, RUB-20b) or 59% (RUB-40). In order to rationalize these findings a modified structure model with partly interrupted Si5-O12-Si5 groups had to be postulated. The connectivity analysis of the fer-type layer shows that the ideal, non-interrupted fer-layer has four Q^3 -type and fourteen Q^4 -type SiO_4 tetrahedra per 2-dimensional unit cell, the Q^4 / Q^3 ratio is 3.5. If all Si5-O12-Si5 bonds are broken and replaced by Si-OH groups the Q^4 / Q^3 ratio changes to 1.25 with eight Q^3 -type and ten Q^4 -type SiO_4 tetrahedra (see Fig. 1 and Tab. 5). Complementary to the Rietveld structure analysis the information on the actual Q^4 / Q^3 ratio can be obtained from solid-state ^{29}Si MAS NMR spectroscopy. The ^{29}Si MAS NMR spectra of RUB-20, RUB-20b and RUB-40 revealed Q^4 / Q^3 ratios of 2.0 to 2.4 instead of the expected ratio of 3.5 for a perfect fer layer. This reflects a considerable amount of defects within the fer layer. In the case of RUB-20, -20b and -40 the structure analysis showed that the defects are not randomly distributed throughout the layer structure but involve only the Si5-O12-Si5 group.

To evaluate in particular the local structure around the Si5 site, the structures of RUB-20, RUB-20b and RUB-40 were refined based on two different starting models:

- 1) Assuming a fer layer without defects (the O12 site is completely occupied and all Si5-O12 bonds are present) and assuming that the additional electron density peak close to Si5 is a water molecule.

This structure model is close to the related materials PLS-1¹⁰ and ERS-12¹³ which had been refined under these assumptions. The structure model based on the non-interrupted layer (in P2₁/m) contains 6 independent Si sites (with 18 Si atoms in total per unit cell), 12 independent oxygen sites (with 38 O atoms in total per unit cell), one TMA/TMP site (2-fold) and one water site (2-fold).

The refinements led to:

RUB-20: $\chi^2 = 5.1$, $R_{\text{Bragg}} = 0.052$, $R_{\text{wp}} = 0.103$, $d(\text{Si5-O12}) = 2.06(2)$ Å, $\text{occ.}(\text{O12}) = 100\%$

RUB-20b: $\chi^2 = 5.3$, $R_{\text{Bragg}} = 0.054$, $R_{\text{wp}} = 0.104$, $d(\text{Si5-O12}) = 2.04(2)$ Å, $\text{occ.}(\text{O12}) = 100\%$

RUB-40: $\chi^2 = 2.8$, $R_{\text{Bragg}} = 0.079$, $R_{\text{wp}} = 0.172$, $d(\text{Si5-O12}) = 1.83(1)$ Å, $\text{occ.}(\text{O12}) = 100\%$

2) Assuming a fer layer with ordered defects (the O12 site is only partly occupied, the former Si-5 site is split into Si51 forming the Si51-O12-Si51 bonds and Si52 forming the two Si52-OH2 groups) and assuming that the additional electron density peak close to Si52 is an OH group.

This improved structure model now contains 7 independent Si sites (with still 18 Si atoms in total per unit cell), 13 independent oxygen sites (with 39 O atoms in total per unit cell), one TMA/TMP site (2-fold) but no water. The refinements led to:

RUB-20: $\chi^2 = 3.1$, $R_{\text{Bragg}} = 0.033$, $R_{\text{wp}} = 0.088$, $d(\text{Si5-O12}) = 1.57(2)$ Å, $d(\text{Si52-OH2}) = 1.57(3)$ Å, $\text{occ.}(\text{O12}) = 53\%$

RUB-20b: $\chi^2 = 3.9$, $R_{\text{Bragg}} = 0.032$, $R_{\text{wp}} = 0.078$, $d(\text{Si5-O12}) = 1.55(2)$ Å, $d(\text{Si52-OH2}) = 1.60(3)$ Å, $\text{occ.}(\text{O12}) = 50\%$

RUB-40: $\chi^2 = 1.9$, $R_{\text{Bragg}} = 0.051$, $R_{\text{wp}} = 0.144$, $d(\text{Si5-O12}) = 1.59(2)$ Å, $d(\text{Si52-OH2}) = 1.62(3)$ Å, $\text{occ.}(\text{O12}) = 59\%$

The results clearly indicate that the structure model based on fer layers with ordered defects is significantly better than the former model and is valid for RUB-20, RUB-20b and RUB-40.

As an example of the monoclinic materials the structure of RUB-40 will be discussed in more detail:

The fer layers are stacked in an AAA sequence yielding a crystal lattice of monoclinic symmetry with an angle β of 99.3°. The shift vector between successive layers is $1 a_0 + 0 b_0 \pm 0.24 c_0$. See Figure 13 (left) for the arrangement of layers. The silicate layers are built by seven symmetrically independent Si atoms and 19 independent oxygen atoms in the structure. As mentioned above some Si5-O12-Si5 bridges are interrupted with the result that the ideal Si5 atom now occupies split positions (Si51, Si52).

The occupancy factor of O12 was refined to 0.59(1) which means that ca. 40 % of the Si5-O12-Si5 groups are replaced by two Si52-OH2 groups. This leads to 5.6 Q³-type and 12.4 Q⁴-type SiO₄ tetrahedra per unit cell with a Q⁴ / Q³ ratio of 2.2. (Corresponding values of RUB-20 and RUB-20b are: Q⁴ / Q³ = 2.0). A Q⁴ / Q³ ratio of 2.2 is in very good agreement with the value determined from the ²⁹Si MAS NMR spectrum of RUB-40 (Q⁴ / Q³ = 2.3, see Table 5).

Concerning the arrangement of inter-layer hydrogen bonds, it is instructive to compare the structures of RUB-40 and RUB-36: RUB-36 (like RUB-38 and RUB-48) possesses only isolated inter-layer hydrogen bonds between the silanol/siloxy groups of neighbouring layers (Fig. 10). The presence of additional Si52-OH2 groups in RUB-40 leads to a more complex system of hydrogen bonds. As shown in Figure 12 (bottom) the interaction between the “regular” silanol/siloxy groups (O6, O6') is complemented by strong hydrogen bonds between O6 and OH2. The distance between (O6...O6') is 2.55(3) Å while the distance between O6 and OH2 is 2.31(4) Å. These distances correspond approximately to the distances as calculated from the chemical shift values of the ¹H MAS NMR signals of RUB-40 (compare Table 6). The existence of these clusters of hydrogen bridges in RUB-40 with a larger number of hydrogen bonds compared to the structures of RUB-36, -38 and -48 should lead to stronger interaction between the neighbouring silicate layers.

Intercalated between the fer layers there are two tetramethylphosphonium cations (TMP) per unit cell. No water was detected in the inter-layer region. Figure 12 (bottom) depicts a projection of the structure with the orientation of the tetramethylammonium cations inside the pores. The organic cations are isolated from one another, but v.d.Waals contacts exist between the methyl groups of the cation and oxygen atoms of the silicate layer. Atomic coordinates, displacement parameters, occupancy factors as obtained from the Rietveld refinement as well as bond lengths, bond angles and distances of RUB-40 are provided as Supplementary Info (cif file).

The structures of **RUB-20 and RUB-20b** are very similar to that of RUB-40. The use of the tetramethylammonium cation as a structure director leads to a very similar structural arrangement of fer layers and cations as observed for RUB-40. Crystal structure data including interatomic distances and bond angles are provided as Supplementary Info (cif file).

The shift vector between successive layers is $1 a_0 + 0 b_0 \pm 0.19 c_0$. It deviates somewhat from the shift vector calculated for RUB-40 probably because of the smaller size of the TMA cation. The inter-layer distances along the a-axis, $d_{L-L} = 10.4 \text{ \AA}$ (RUB-20) and 10.5 \AA (RUB-20b), however, are very similar to the value of RUB-40 ($d_{L-L} = 10.6 \text{ \AA}$).

In the case of RUB-20 and -20b the same type of clustered inter-layer hydrogen bonds exist between terminal silanol/siloxy groups with O...O-distances between 2.3 and 2.5 Å. Thus, the larger SDA in RUB-40 is accommodated by the slightly different stacking arrangement (= different shift vector) and not by an increased interlayer distance which would have weakened the hydrogen bonding directly.

Our structure analysis of the three different samples containing the fer layer and TMA as SDA unanimously show that the presence of interrupted fer layers in HLSs is not a peculiarity of one particular sample but seems to appear systematically in HLSs synthesized with specific SDAs (see the discussion section below). All three monoclinic samples investigated here showed the same structure with fer layers containing ordered defects in the silicate layer.

Analysing the published literature, there are indications that the silicate layers of PLS-1 and ERS-12 as well possess interrupted Si-O-Si groups to a certain extent. The structure of ERS-12 has a significant larger Si5-O12 distance (1.776(30) Å) than all other Si-O distances (1.580(6) – 1.638(6) Å), The structure of PLS-1 possesses also an electron density maximum close to Si5 which in that study was assigned to be a potassium cation. The distance of this cation to the Si5 atom (= 1.51(2) Å), however, is unusually short.

In the case of RUB-20 and RUB-20b additional Rietveld refinements indicate that the structures are best to be described based on the non-centric space group $P2_1$. This increases the number of Si sites to eleven and also the number of variables to be refined. The resulting geometries of the structures are almost identical, convincing us to report the details of the averaged, higher symmetrical structure.

Comparison of layer silicates being composed of fer layers

So far, about 20 different HLSs with fer layers have been reported in the literature - including the materials of this study. They differ from each other with respect to i) the organic cations residing between the silicate layers, ii) the arrangement of neighbouring fer layers relative to each other and iii) the amount of ordered defects in the layer (leading to different Q3 : Q4 - ratios of the Si atoms of the layer)

Organic cations

HLS structures with fer layers are very flexible to incorporate various organic cations. The cations residing between fer layers differ both chemically and geometrically. The cations comprise

alkylammonium (e.g. tetraethylammonium), alkylphosphonium (e.g. tetramethylphosphonium), hydroxyalkylammonium (e.g. hydroxoethyltrimethylammonium) and aromatic (Diquat-4) compounds (see Tables 1 and 2). They are predominantly monovalent but also divalent cations have been observed (tetramethylen-bis(N- methyl)-pyrrolidinium and Diquat-4). The cations differ also considerably with respect to their molecular geometry. They can be nearly isometric like quinuclidine, chain-like as tetramethylen-bis(N-methyl)-pyrrolidinium, branched like tetraethylammonium or cyclic with sidegroups (4-amino-2,2,6,6- tetramethylpiperidine). Such a variety of cations has not been observed for HLSs of any other layer type. Moreover, also water molecules can be an important part of the HLS structure (e.g. PREFER)

Layer arrangement

A comparison of all structurally investigated layer silicates with fer layers is presented in Figure 13. The organic cations are omitted for clarity.

Four different layer arrangement types, named MONO-1, ORTHO-1, ORTHO-2 and ORTHO-3, have been reported so far (see Table 8). These types are characterized by different shift vectors between neighbouring layers (the a-axis represents always the stacking direction). The first arrangement type which leads to monoclinic structures (**MONO-1**) is stacked in an AAA-sequence, has one layer per unit cell and is described by a general shift vector: $\mathbf{1 a}_0 + \mathbf{0 b}_0 + \mathbf{z c}_0$. The variable z can embrace different values depending on the size and geometry of the cation (Tab. 8).

All orthorhombic materials possess stacking sequences ABAB and, therefore, possess two layers per unit cell. For these materials three different arrangement types with distinct shift vectors can be defined: The arrangement types are described as follows:

ORTHO-1: $\frac{1}{2} \mathbf{a}_0 + \frac{1}{2} \mathbf{b}_0 + \frac{1}{2} \mathbf{c}_0$

ORTHO-2: $\frac{1}{2} \mathbf{a}_0 + \mathbf{0 b}_0 + \frac{1}{2} \mathbf{c}_0$ and

ORTHO-3: $\frac{1}{2} \mathbf{a}_0 + \mathbf{0 b}_0 \pm \mathbf{z c}_0$,

The value of z is variable and depends on the size and geometry of the cation being included in the structure (see Table 8).

On the left hand side of Figure 13 the monoclinic layer arrangement type is shown. The inter-layer hydrogen bonds between the terminal silanol groups of neighbouring silicate layers are highlighted as blue dotted lines since the hydrogen bonds are most important for the stability of the materials. The O...O distances of the inter-layer hydrogen bonds vary somewhat between 2.6 and 2.8 Å depending on the particular composition of the material. The corresponding values for ERS-12 ad PLS-1 are taken from the literature and are included for comparison (for all structures reported by other groups the values are taken from the publications or calculated from the atomic

coordinates given in the publication). In any case, the hydrogen bonds of the monoclinic materials are weaker than those determined for the orthorhombic silicates which have quite strong bonds. The first orthorhombic arrangement type, ORTHO-1, is represented by PLS-3 and PREFER. For PLS-3 the O...O distance of the interlayer hydrogen bonds was determined to 1.93 Å (based on a Rietveld refinement) and 2.4 Å (from ^1H NMR spectroscopy).^{15a}

An exception among the orthorhombic materials is PREFER which has a rather large interlayer distance $d_{\text{L-L}} = 13.7$ Å because of the big organic cations residing between the layers. This precludes the presence of direct hydrogen bonds between silanol groups of neighbouring layers. Heating of PREFER nevertheless results in the formation of highly ordered Ferrierite. In the case of PREFER additional water molecules are probably part of a hydrogen bonding system. Unfortunately, the structure model does not give information on such details.³⁷

The second arrangement type, ORTHO-2, has a different stacking of the layers. As can be seen in the upper projection (Figure 13) every second layer is shifted by half a unit cell along the b- and the c-axis. Three materials, MCM-47, MCM-65 and RUB-38, are known to have this arrangement of fer layers. All three silicates have rather strong inter-layer hydrogen bonds with O...O distances of ca. 2.4 Å

The third arrangement type, ORTHO-3, also shows a shift of every second layer by $\frac{1}{2} b_0$ (upper projection in Fig. 13) but in contrast to ORTHO-2 the shift along the c-axis deviates from $0.5 c_0$ and varies in the range of $\pm 0.32 c_0$ to $\pm 0.39 c_0$ (lower projection in Fig. 13). This type of shift leads to structures of lower symmetry compared to arrangement type ORTHO-2 (a primitive unit cell is generated instead of a B-centered one) Four materials, RUB-36, RUB-48, UZM-13 and PLS-4 are known to have this arrangement of fer layers. Similar to the materials of type ORTHO-2 these silicates as well have strong inter-layer hydrogen bonds with O...O distances of ca. 2.4 Å.

Defects

For the first time HLSs with systematically interrupted silicate layer were observed (RUB-20 and RUB-40). Because only a part of the Si5-O12-Si5 groups are disrupted the topology of the layer is still regarded to be of the fer type. So far, only the cations TMA and TMP led to the formation of interrupted fer layers while other (larger) cations formed HLSs with non-interrupted fer layers. The interrupted layers have a higher max. charge density than the perfect fer layer and form additional hydrogen bridges between neighbouring layers (see Fig. 12, right and General Discussion section).

Framework silicates

Synthesis by topotactic condensation of hydrous layer silicates

Typically, Hydrous Layered Silicates (HLSs) contain complete silicate layers without defects or with a negligible amount of defects.⁸ The only exceptions known so far are RUB-20, RUB-20b and RUB-40 which contain a considerable amount of ordered defects of the Si-OH type.

In principal, the HLSs can be condensed at a temperature of ca. 400-600°C via a topotactic condensation of neighbouring Si-OH groups according to the reaction $\equiv\text{Si-OH} + \text{HO-Si}\equiv \rightarrow \equiv\text{Si-O-Si}\equiv + \text{H}_2\text{O}$. If all inter-layer cations are removed during the condensation process, and if only defect-free layers are present an uninterrupted microporous silica framework can be produced. With the exception of RUB-40 (containing tetramethylphosphonium ions) the layered RUB materials investigated here contain only alkylammonium compounds as inter-layer cations which were completely removed during condensation by heating (see thermal analysis, Table 7); consequently, nominally neutral SiO₂ frameworks are generated. The orthorhombic layered RUB materials possess non-interrupted fer layers. Still, although the hydrous layer silicates used as precursors are of moderate to good crystallinity, the condensation of layers occurs not always in a periodic way but a random condensation of Si-OH groups is possible as well. As indicated by powder XRD experiments, diffraction diagrams show broadened reflexions, indicating that the formation of a disordered framework structure occurs quite frequently. In some cases only a few very broad reflexions are detected showing that a highly disordered framework structure has formed (Fig. 14). The monoclinic layered RUB materials, however, are unlikely to produce defect-free SiO₂ frameworks because the silanol groups of the interrupted silicate layer can not directly react with a neighbouring silanol group for geometric reasons: the additional Si5-OH₂ groups point in opposite directions, so they cannot be condensed to “reestablish” the Si5-O12-Si5 bridge.

Characterization of the framework silicates

Powder XRD

The condensation process is, in general, clearly detectable from the X-ray powder diffraction patterns. The topotactic condensation leads to a shrinking of the unit cell along the stacking direction of layers while the other unit cell parameters remain virtually unchanged. In Figure 15 the pattern of the layered precursor RUB-36 is compared with the one of the corresponding zeolite RUB-37 (zeolite framework type CDO). The first strong peak of each pattern reflects the distance between neighbouring silicate layers and clearly confirms the reduction during the condensation process (in this case from 11.1 Å to 9.2 Å). Although there are considerable structural changes during the condensation the plate-like morphology of the crystals is maintained (Fig. 3, bottom).

The random condensation leads to a highly disordered material. As can be seen from Figure 16 the product obtained from heating RUB-40 shows a powder pattern with only a few very broad peaks indicative of very low crystalline order.

Using the peak halfwidths as a measure to assess the degree of structural order it is obvious that the calcined RUB-36 (= “well ordered RUB-37”) has the highest crystallinity of all five calcination products. The high crystallinity of the RUB-37 material derived from diethyldimethylammonium containing RUB-36 as a precursor is also reflected by the fact that RUB-37 has a high BET surface area of 334 m²/g and a large pore volume of 0.22 cm³/g.³⁸ This indicates a well ordered structure without defects like stacking disorder or random condensation which might block the pore system. The calcination of the other two orthorhombic materials RUB-38 and RUB-48 led to “fairly ordered RUB-37” while the heating of the monoclinic materials RUB-20 and RUB-40 formed “poorly ordered RUB-37” and a highly disordered material, respectively.

NMR spectroscopy

Solid state NMR spectroscopy, as well, is very suitable to investigate the structural changes occurring during the condensation reaction. It especially answers the question whether the condensation of the silicate framework is complete. The broadness of the signals gives an indication on the degree of structural order.

As an example the phyllo/tecto pair RUB-36/RUB-37 is described here. The ²⁹Si MAS NMR spectrum of the layer silicate RUB-36 shows signals in the ranges between -96 to -104 ppm (Q³-type silicon) and -104 to -116 ppm (Q⁴-type silicon). The ²⁹Si MAS NMR spectra of the corresponding zeolite RUB-37 present only one broad signal centered in the Q⁴-region at ca. -112 ppm indicating that most Si atoms are four-connected to neighbouring Si atoms (Fig. 17).

Structure analysis

Only the well ordered RUB-37 sample obtained from RUB-36 as the precursor was structurally analyzed by a Rietveld analysis of X-ray powder diffraction data. As a starting model for the structure refinement, the atomic coordinates of CDO-type materials as published on the website of the IZA was used.²⁶ The refinement was performed based on the centric space group Bbmm (no. 63) as well as the acentric space group Bb₂1m (no. 36). For the given topology of the framework the high symmetry of space group Bbmm requires that two Si-O-Si angles are straight (Si₂-O₆-Si₂ = 180° and Si₃-O₈-Si₃ = 180°). It can be assumed that the refined position of the oxygen atom bridging the Si atoms represents a space and/or time average of many different oxygen positions deviating slightly from the 180°-straight Si-O-Si bridge. This, as compensation, leads to some very short bonds: d(Si₂-O₆) = 1.48 Å and d(Si₃-O₈) = 1.55 Å. A refinement of the RUB-37 structure in

the acentric space group Bb2₁m lead to a significant improvement. The Si-O-Si angles around O6 and O8 decreased to 154° and 162°, respectively, but still, some the Si-O bond lengths remained unusually short (shortest: d(Si2-O6) = 1.53(3) Å). Difference Fourier maps after the refinement of the framework atoms showed no significant electron density in the channel like voids. The channel voids are free of matter, i.e. the DEDMA cations of the precursor were expelled during the condensation process upon heating.

Since RUB-37 is a silica zeolite of framework type CDO it has a very similar structure to other CDO-type zeolites CDS-1,¹⁰ UZM-25,¹⁶ calcined MCM-65¹² and possibly to calcined ERS-12.¹³ Crystal structure data including interatomic distances and bond angles are provided as Supplementary Info (cif file, refinement in spacegroup Cmc2₁ (standard setting)).

General Discussion

The structure analyses and the general characterization of a series of closely related materials shed light on fundamental questions concerning the synthesis of HLSs and concerning the synthesis of zeolites via topotactic condensation.

What are favourable synthesis conditions to form HLSs with fer layers?

The fer layer seems to be a building unit for a number of HLSs which forms preferentially if a reaction mixture of the simple composition SDA – SiO₂ – water is heated to medium synthesis temperatures (150 – 180°C). As mentioned above (Tab. 1), fer layers form under hydrothermal conditions from aqueous solutions of silicic acid and a surprisingly large number of different SDAs. The different SDAs are accommodated between neighbouring layers optimizing bonding interactions with the layer surface.

Other layer types like the heu layer in RUB-39³⁵ or the ast layer in HUS-1³⁹ and β-Helix-Layered-Silicate⁴⁰ are reported for only one particular SDA - dimethyldiropylammonium in the case of heu and TMA in the case of the ast layer. The cas layer for example has so far been reported for two SDAs – piperazinium (forming EU-19)²⁰ and 4,4-bipyridine (forming NU-6(1))²². In contrast, for HLSs containing the fer layer there is no obvious templating effect of the cation added to the synthesis mixture. Consequently, fer layers are formed with a large variety of cations possessing different sizes and geometries (Table 1).

The synthesis temperature, however, seems to play an important role for the formation of fer layers (see synthesis temperatures in Table 1).

The use of diethyldimethylammonium cations, for example, results in the crystallization of RUB-56 at 120-140°C (unknown structure),⁴¹ RUB-52 at 130°C (layer type r52)⁴² but leads to the formation of UZM-13,¹⁶ PLS-4^{15a} and RUB-36 (all containing fer layers) at 150°C - 170°C.

The use of tetramethylammonium (TMA) generates a HLS with sod layers (RUB-15 at low synthesis temperatures of ca. 120 – 140°C⁴³) or to two different HLSs with ast layers (HUS-1 at 125°C³⁹ and RUB-55 at 160°C⁴⁴). Only at a moderate temperature of ca. 160°C-180°C RUB-20 and the closely related material ERS-12¹³ crystallize from the reaction mixture. This observation of the temperature dependence of product formation seems to be correlated to the Q^3 / Q^4 ratios of the different layer types being present in the structure of the HLSs:

In the case of materials formed with diethyldimethylammonium as the SDA the following Q^3 / Q^4 ratio are observed: RUB-56 = 1 : 1; RUB-52 = 1 : 1.5, RUB-36 = 1 : 3.5. In the case of tetramethylammonium a similar order arises: RUB-15 = 1 : 0.5, HUS-1 = 1 : 0.25, RUB-55 = 1 : 0.25, RUB-20 = 1 : 3.5. This might indicate that at relatively high synthesis temperature layer types are stabilized that possess a higher content of Q^4 -type silica, i.e. are condensed to a higher degree. To validate this “rule” more successful synthesis experiments are needed.

Which structural features of the layered precursor determine the quality of the resulting framework silicate?

- The quality of the framework silicates as product of the topotactic condensation is determined by
- the degree of order reflected in the stacking of layer-like building units in the framework structure (does stacking disorder occur?),
 - the completeness of condensation (is the condensation incomplete with remaining silanol groups?).
 - the degree of order concerning the formation of Si-O-Si bridges (is there a random condensation with arbitrary orientation of Si-O-Si bridges and/or is there intra-layer condensation?).

Five different structural features of the HLSs will be considered which might have an influence on the crystallinity of the framework silicates formed by topotactic condensation.

Topology of the layer structure

As already mentioned in Section 2 the terminal silanol ($\equiv\text{Si-OH}$) or siloxy ($\equiv\text{Si-O}^-$) groups of the fer layer have a rather large distance of at least 5.7 Å from each other. It is, therefore, unlikely that

an intra-layer condensation of these groups occurs if such a material is heated. Instead, inter-layer Si-O-Si bridges are likely to be generated leading to a complete and ordered framework. This is different to other layers like e.g. the kan, sod, or rwr layers which have short intra-layer hydrogen bonds of a length of ca. 2.5 Å.⁸ During heating the corresponding silanol ($\equiv\text{Si-OH}$) or siloxy ($\equiv\text{Si-O}$) groups are likely to form Si-O-Si bridges within a layer and by that generate an interrupted or highly distorted framework. In order to avoid intra-layer condensation the silanol groups of the layer should have a distance of more than ca. 4 Å from each. This is fulfilled in the case of the fer layer.

Real structure of the layer

As has been shown in this study some HLSs contain fer layers with ordered defects (RUB-20, RUB-20b and RUB-40). The presence of defect silanol groups Si5-OH2 in addition to the regular silanol/siloxo groups Si1-O6 increases the chance of random inter-layer condensation of silanol groups. The possibility to establish connections of Si5 and Si1 of a given layer with either Si5 or Si1 of the neighbouring layer makes it very likely that a disordered structure is generated during the condensation process. Therefore, it is very likely to produce a condensation product of low crystallinity and poor porosity. This has been shown for the condensation products of RUB-20 and RUB-20b.

In contrast, the orthorhombic materials RUB-36, -38 and -48 which have non-interrupted fer layers form condensation products of moderate to good crystallinity.

Hydrogen bonds

The inter-layer hydrogen bonds contribute significantly to the stability of the precursor material and keep the layers at the appropriate position in the structure. In general, the orientation of the hydrogen bond (Si-OH---HO-Si) within the precursor structure is nearly identical to the orientation of the Si-O-Si bond in the silicate framework being formed during the condensation process.

With the exception of PREFER the inter-layer hydrogen bonds of the orthorhombic phases are very strong ($d_{\text{O}\dots\text{O}} \approx 2.2 - 2.5 \text{ \AA}$). Although RUB-36, RUB-38, RUB-48, MCM-47 and UZM-13 have the same number of hydrogen bonds per unit cell with bonds of similar strength the resulting framework silicates are of different quality. The absolute strength of the hydrogen bond seems to be less important: MCM-47 ($d_{\text{O}\dots\text{O}} = 2.23 \text{ \AA}$) is transformed into a fairly ordered CDO-type zeolite¹¹ while UZM-13 ($d_{\text{O}\dots\text{O}} = 2.54 \text{ \AA}$) is condensed to a well ordered CDO-type zeolite.¹⁶

The monoclinic materials possess strong to medium strong hydrogen bonds (see Table 6). However, the monoclinic structures are not included in the discussion concerning hydrogen bonds because it is believed that the defects of the silicate layer dominate by far the condensation process with respect to the crystallinity.

We can conclude that inter-layer hydrogen bonds predetermine the stacking sequence of the layer-like building units (FER-type or CDO-type). Whether a framework silicate of higher or lower degree of structural order is formed is not directly related to the strength of the hydrogen bonds.

Layer stacking

In many cases the silicate layers can be stacked in two or more different ordered sequences which all allow for short inter-layer hydrogen bonds. This is also true for the fer layer which can be stacked in to two different stacking sequences (see Figure 2). The inter-layer hydrogen bonds predetermine the position of the Si-O-Si bonds being formed during the condensation process. If the structure of the layered precursor has already a stacking disorder of layers (randomly varying shift vectors) it is nearly inevitable that this disorder will be inherited by the framework silicate formed by the condensation. To obtain a zeolite with a highly ordered framework structure via topotactic condensation of a layered precursor it is, therefore, a prerequisite that the layered precursor has already a highly ordered structure.

The exact values of the stacking vector components have seemingly no significant influence on the quality of the CDO-type zeolite being formed through topotactic condensation. If one compares the structures of the orthorhombic precursor materials with shift vector $0.5 a_0 + 0 b_0 + z c_0$ (see Fig. 13, Table 8) z adopts different values for PLS-3 ($z = 0.32$), RUB-36 ($z = 0.36$), UZM-13 ($z = 0.38$), RUB-48 ($z = 0.39$), RUB-38 ($z = 0.5$), MCM-65 ($z = 0.5$) and MCM-47 ($z = 0.5$). A value of $z = 0.5$ (RUB-38, MCM-47, MCM-65) means that the fer layers are separated from each other only along the a -axis and the layers need only to move towards each other along the stacking axis a (see Fig. 13). The condensation of layers from requires an additional small layer shift along the b -axis to form the CDO-type zeolite. The layer arrangement all other materials requires that the silicate layers not only approach each other but also have to move slightly along the b axis to facilitate the condensation into the orthorhombic CDO-type framework. Nevertheless, among the materials discussed here, only RUB-36 and UZM-13 are transformed into framework silicates of high structural order although their shift values deviate from $z = 0.5$.

Type of cation

Among the materials investigated in this study, the heating of RUB-36 led to the framework with highest degree of structural order. A similar observation was reported by Knight et al. who investigated a series of fer-layer silicates with cations diethyldimethylammonium (UZM-13), ethyltrimethylammonium (UZM-17) and diquat-4 (UZM-19).¹⁶ Also among this group of materials, UZM-13 containing the diethyldimethylammonium cation led to the condensation product with highest structural order. Ikeda et al. mention in their paper that PLS-4, a structural analogue of RUB-36 “can be easily converted to the topotactic CDO-type zeolite structure by calcination”.^{15a} There is, however, no information on the crystallinity of the CDO-type zeolite. PLS-4 contains diethyldimethylammonium and possesses the same layer arrangement as RUB-36, but has a slightly reduced symmetry, $P2_1/c$, with a monoclinic angle of $89.80(2)^\circ$.

For a given layer topology the intercalated cation plays the key role for a successful condensation of the layered precursor into a well ordered framework. It can be assumed that a suitable organic compound (e.g. the cation itself or a decomposition product) is necessary to keep the silicate layers in place until the topotactic condensation has at least started. A similar conclusion concerning the conversion of hydrous layered silicates has already been presented by Oumi et al.⁴⁵ The size of the cation determines the interlayer distance and, therefore the strength of the hydrogen bonds. Moreover, in some cases the silicate layers have to slide a short way into appropriate position.

In addition, a suitable thermal stability - or better “instability” - of the cation is important. Typically, the terminal silanol groups of the silicate layers of as-made HLSs are separated from each other by a distance of ca. 2 to 3 Å. For a successful condensation of silanol groups the cation should not prevent the movement of neighbouring layers towards each other. At about the same temperature at which the condensation takes place the cation has to be destroyed and expelled to give way for the converging layers. Most likely, the process will start from the rim of the crystal removing the SDA closest. In a consecutive step the condensation might take place. In order to arrange the stacking only two inter-layer Si – O – Si bridges have to be generated, then the orientation of the layers with respect to each other is fixed.

Alkylphosphonium cations are not suitable for a successful condensation of HLSs. As can be seen from Table 7 the burn off of the tetramethylphosphonium cation in RUB-40 indicated by the exothermic peak happens at ca. 548°C which is about 100°C higher than the corresponding temperatures of the ammonium cations and does not coincide with the beginning of the

condensation. Moreover, the phosphonium cation can not completely be expelled from the structure probably because it is oxidized to a phosphate group.

To obtain a zeolite with a highly ordered structure it seems to be a prerequisite that a suitable cation is intercalated between the layers of the precursor which has a suitable (small) size to allow for strong inter-layer hydrogen bonds and to keep the layers in place until the condensation has started, but also possesses a suitable thermal (in)stability to allow the condensation process to proceed.

Conclusion

Several new Hydrous Layer Silicates possessing fer layers have been synthesized and were structurally analyzed in this study. It is shown that the organic SDAs play a similar role in the structure directing process of HLS as in zeolite synthesis. The different materials presented in this study all having the fer layer as silicates layer demonstrates the surprising flexibility of this synthesis system. It also stimulates the search for new structures exploiting the SDA based synthesis principles more systematically. The set of rules and conclusions drawn from the comparison of the different structures provides a new basis for HLS research. For the first time also some HLSs with interrupted silicate layers were observed. RUB-20 and RUB-40 possess a high density of ordered defects which is unique among the HLSs with known structure.

The successful synthesis of the well ordered CDO-type zeolite (RUB-37) is another example for the potential of this new zeolite synthesis route employing the topotactic condensation of layered precursors. The topotactic condensation of Hydrous Layer Silicates opens up an interesting way to form new zeolite materials with novel framework types which may not be obtained by other synthesis routes. The structure of the parent materials is a key feature for the preparation of well crystalline zeolites. This study gives some insights which features are favourable to prepare well crystalline zeolites via topotactic condensation. Among the HLSs containing fer layers, RUB-36 is the material of highest potential. RUB-36 can be heated to form a well ordered CDO-type zeolite, named RUB-37 which is superior to the condensation products obtained from the other precursor materials.

Acknowledgements

The authors would like to thank Dr. Carsten Bähz (Hasylab, Hamburg) for collecting the synchrotron diffraction data and Dr. Michael Fechtelkord for running the NMR spectra. Very instructive comments of two anonymous referees are gratefully acknowledged.

Keywords:

hydrous layer silicate, Ferrierite-type layer, CDO, structure, synthesis, fer, ordered defects.

Reverences

- 1 H. Gies, U. Mueller, B.Yilmaz, T. Tatsumi, B. Xie, FS. Xiao, XH. Bao, WP. Zhang, D. de Vos, *Chem. Mater.*, 2011, **23**, 2545.
- 2 S. Inagaki, Y. Sakamoto, Y. Fukushima and O. Terasaki, *Chem. Mater.*, 1996, **8**, 2089
- 3 A. Corma, V. Fornes, J. Martinez-Triguero and S.B. Pergher, *J. Catalysis* 1999, **186**, 57.
- 4 A. Corma, U. Diaz, M.E. Domine and V. Fornes, *J. Amer. Chem. Soc.*, 2000, **122**, 2804.
- 5 A. Corma, V. Fornes, U. Diaz, *Chem. Commun* **24**, 2001, 2642.
- 5a A. Corma, U. Diaz, M.E. Domine and V. Fornés, *Angew. Chem. Int Ed.*, 2000, **39**, 1499.
- 6 M.E. Leonowicz, J.A. Lawton, S.L. Lawton and M.K Rubin., *Science*, 1994, **264**, 1910.
- 7 L. Schreyeck, P. Caullet, J.C. Mougénel, J.L. Guth and B. Marler, *Microporous Mater.*, 1996, **6**, 259.
- 8 B. Marler and H. Gies, *Eur. J. Mineral.*, 2012, **24**, 405.
- 9 S. Vortmann, J. Rius, S. Siegmann, and H. Gies, *J. Phys. Chem. B*, 1997, **101**, 1292.
- 10 T. Ikeda, Y. Akiyama, Y. Oumi, Y. Kawai and F. Mizukami, *Angew. Chem. Intern. Ed.*, 2004, **43**, 4892.
- 11 A. Burton, R.J. Accardi and R.F. Lobo, *Chem. Mater.*, 2000, **12**, 2936.
- 12 D.L. Dorset and G.J. Kennedy, *J. Phys. Chem. B*, 2004, **108**, 15216.
- 12a S.S. Dhingra, C.T. Kresge and S.G. Casmer, 2005, *US Patent* 6,869,587.
- 13 R. Millini, L.C. Carluccio, A. Carati, G. Bellussi, C. Perego, G. Cruciani and S. Zanardi, *Microporous Mesoporous Mater.*, 2004, **74**, 59.
- 14 K. Yamamoto, T. Ikeda, M. Onodera and A. Muramatsu Book of Abstracts, 15th International Zeolite Conference, Beijing, 2007, 452.
- 15 T. Ikeda, S. Kayamori, T. Hanaoka and F. Mizukami, Book of Abstracts, 15th International Zeolite Conference, Beijing, 2007, 589.
- 15a T. Ikeda, S. Kayamori and F. Mizukami, *J. Mater. Chem.*, 2009, **19**, 5518.
- 16 L.M. Knight, M.A. Miller, S.C. Koster, M.G. Gatter, A.I. Benin, R.R. Willis, G.J. Lewis and R.W. Broach, in "Studies in Surface Science and Catalysis, Vol. 170, FROM ZEOLITES TO POROUS MOF MATERIALS" (Eds.: R. Xu, Z. Gao, J. Chen, W. Yan), 2007, 338.
- 17 P. Chu, G.W. Kirker, S. Krishnamurthy and J.C. Vartuli, *US Patent* 4,985,223, 1991.
- 18 M.K. Rubin, *US Patent* 5,063037, 1991.
- 19 Y. Asakura, R. Takayama, T. Shibue and K. Kuroda, *Chem. Eur. J.*, 2014, **20**, 1893.
- 20 A.J. Blake, K.R. Franklin and B.M. Lowe, *J. Chem. Soc. Dalton Trans.*, 1988, 2513.
- 20a B. Marler, M.A. Camblor and H. Gies, *Microporous Mesoporous Mater.* 2006, **90**, 87.
- 21 A. Rojas and M.A. Camblor, *Chem. Mater.*, 2014, **26**, 1161.
- 22 S. Zanardi, A. Alberti, G. Cruciani, A. Corma, V. Fornes and M. Brunelli, *Angew. Chem. Intern. Ed.*, 2004, **43**, 4933.
- 23 Y.X. Wang, H. Gies, B. Marler and U. Müller, *Chem. Mater.*, 2005, **17**, 43.
- 24 B. Marler, N. Ströter and H. Gies, *Microporous Mesoporous Mater.*, 2005, **83**, 201.
- 25 T. Moteki, W. Chaikittisilp, A. Shimojima and T. Okubo, *J. Am. Chem. Soc.*, 2008, **130**, 15780.
- 25a H. Voss, J. Therre, H. Gies and B. Marler, 2010, *International Patent* WO/2010/037690 A1, Application No.: PCT/EP2009/062479
- 26 C. Baerlocher, L.B. McCusker, and D.H. Olson: Atlas of Zeolite Framework Types, 6th Revised Edition, Elsevier, Amsterdam, 2007 and database of Zeolite Structures: <http://www.iza-structure.org/databases/>.
- 27 P. Werner, L. Eriksson, and M. Westdahl, *J. Appl. Crystallogr.*, 1985, **18**, 367.
- 28 T. Roisnel, and J. Rodriguez-Carvajal, <http://cdifx.univ-rennes1.fr/winplotr/winpltr.htm>.

- 29 M.M.J Treacy and J.B Higgins, "Collection of simulated XRD powder patterns for zeolites", Elsevier, Amsterdam (2007).
- 30 J. Rodriguez-Carvajal, *Physica B.*, 1993, **192**, 55; and website <http://www.ill.eu/sites/fullprof/index.html>.
- 31 H. Gies, B. Marler and U. Werthmann, in "Molecular Sieves Science and Technology" (eds. H. G. Karge and J. Weitkamp), 1998, **Vol. 1**, 35, Springer, Berlin.
- 32 G.A. Jeffrey and Y. Yeon, *Acta Crystallogr.* 1986, **42**, 410.
- 33 H. Eckert, J.P. Yesinowski, L.A. Silver, and E.M. Stolper, *Phys.Chem.* 1988, **92**, 2055.
- 34 M. Borowski, O. Kovalev and H. Gies, *Microporous Mesoporous Mater.* 2008, **107**, 71.
- 35 Y.X. Wang, H. Gies and J.H. Lin, *Chem. Mater.*, 2007, **19**, 4181.
- 36 B. Marler and H. Gies, H., Structure and properties of two new TMA silicates with ordered defects: RUB-22, TMA₄[H₁₂Si₃₂O₇₂], a microporous framework material with Si vacancies and RUB-20, TMA₄[H₂Si₁₈O₃₈], a layer silicate with partly hydrolyzed ≡Si-O-Si≡ groups, *In preparation*
- 37 L. Schreyeck, P. Caullet, J.C. Mougénel, J.L. Guth and B. Marler, *Microporous Mater.*, 1996, **6**, 259.
- 38 H. Gies, U. Müller, B. Yilmaz, M. Feyen, T. Tatsumi, H. Imai, H.Y. Zhang, B. Xie, F.S. Xiao, XH. Bao, W. Zhang, T. De Baerdemaeker and D. De Vos, *Chem. Mater.* 2012, **24**, 1536.
- 39 T. Ikeda, Y. Oumi, K. Honda, T. Sano, K. Momma and F. Izumi, *Inorg. Chem.*, 2011, **50**, 2294.
- 40 T. Ikeda Y. Akiyama F. Izumi, Y. Kiyozumi, F. Mizukami and T. Kodaira, *Chem. Mater.*, 2001, **13**, 1286.
- 41 L. Zhang, A. Grünwald-Lüke, B. Marler, Y. Wei and H. Gies, *Book of Abstracts IV Int. Workshop on Layered Materials, Campinas, Brazil*, 2012, **3P15**, p. 139.
- 42 B. Marler, Z. Li, G. Wang, and H. Gies, *Acta Crystallographica Section A*, 2011, **67**, Supplement, C650.
- 43 U. Oberhagemann, P. Bayat, B. Marler, H. Gies and J. Rius, *Angew. Chem. Int. Ed. Engl.* 1996, **35**, 2869.
- 44 B. Marler, A. Grünwald-Lüke, S. Grabowski and H. Gies, *Z. Kristallogr. (Crystalline Materials)*, 2012, **227**, 427.
- 45 Oumi, Y., Takeoka, T., Ikeda, T., Yokoyama, T., Sano, T., 2007, *New J. Chem.* **31**, 593.

Figure Captions

Fig. 1: The *fer* (Ferrierite-type) layer shown in three different projections. Silicon and oxygen atoms are presented as purple and red spheres, respectively; the terminal oxygen atoms of the layer which represent silanol or siloxy groups are displayed as blue spheres.

Fig. 2: *fer* layers can be condensed in two possible ways to form two different ordered silicate frameworks with zeolite framework types FER or CDO.

Fig. 3: SEM micrographs of layer silicates RUB-36 (top, left) and RUB-38 (top, right), and of zeolite RUB-37 (bottom) which was derived from RUB-36 by heating the precursor at 600°C.

Fig. 4: The X-ray powder diagrams of the six layer silicates RUB-20, RUB-20b, RUB-40, RUB-36, RUB-48, RUB-38 from top to bottom. ($\lambda = 1.5406 \text{ \AA}$).

Fig. 5: The solid-state ^{29}Si MAS NMR spectra of RUB-20 (left), and RUB-36 (right) shown here as representatives of the monoclinic and orthorhombic materials, respectively. Signals around -102 ppm can be assigned to Q^3 -type silica while signals around -112 ppm can be assigned to Q^4 -type silica.

Fig. 6: The solid-state ^1H MAS NMR spectra of RUB-20 and RUB-36 shown here as representatives of the monoclinic and orthorhombic materials, respectively. Signals at 1.5 to 3.5 ppm are assigned to protons of methyl and methylene groups, signals between 5.5 and 16.5 ppm indicate hydrogen bonds of different strength.

Fig. 7: DTA (upper) and TG (lower) curves of as made RUB-36 given as an example for the thermal properties of HLSs. Three sections can be distinguished: a) release of physically adsorbed water between 30 and 110°C, b) decomposition and combustion of organic material and generation of water through the condensation of the silicate layers accompanied by an endothermic signal at 373°C and two exothermic signals at 413 and 439°C, c) further loss of organic remains between 440°C and ca. 700°C.

Fig. 8: Plot of the diffraction patterns after Rietveld analysis of RUB-36. Experimental and calculated data are in the upper trace, the difference plot is shown below. Tick marks for allowed reflections are given.

Fig. 9: The structure of RUB-36 presented in two projections: a) along [010] and b) along [001]. Silicon and oxygen atoms are drawn as purple and red spheres, respectively; the terminal oxygen atoms of the layer are displayed as blue spheres. Carbon and nitrogen atoms are displayed in light gray and green colour, respectively. Neighbouring layers show no relative shift in b-direction but a shift of $\pm 0.36 c_0$ in c-direction.

Fig. 10: Section of the inter-layer region of the RUB-36 structure showing the orientation of the diethyldimethylammonium cations inside the "channel-like" voids which are generated by neighbouring silicate layers and hydrogen bonds (blue dotted lines). V.d.Waals contacts between

cation and layer, and between cations themselves are drawn as white and black dotted lines, respectively. Only the shortest contacts are presented in this plot (C-O and C-C \approx 3.4 Å).

Fig. 11: The structure of RUB-38 presented in two projections: a) along [010] and b) along [001].

Silicon and oxygen atoms are presented as purple and red spheres, the terminal oxygen atoms of the layer are displayed as blue spheres. Carbon and nitrogen atoms are displayed in light gray and green colour, respectively. Neighbouring layers show no relative shift in b-direction but a shift of $\pm 0.5 c_0$ in c-direction.

Fig. 12: The structure of RUB-40 presented in a projection along [010]. The upper drawing shows the structure with fer layers without defects: all Si5-O12-Si5 groups are intact and all Si5-O12 bonds are present. The lower drawing presents the structure with partly hydrolyzed Si5-O12-Si5 groups. Each hydrolyzed Si5-O12-Si5 group is replaced by two Si52-OH2 groups pointing towards the TMA cation. OH2-groups take part in the hydrogen bonding network.

Fig. 13: Comparison of all structurally investigated layer silicates with fer layers concerning their layer arrangement. The structure of PREFER is also included. The organic cations are omitted for clarity.

Fig. 14: Powder XRD patterns of the condensation products of RUB-20, RUB-40, RUB-38, RUB-48, and RUB-36 (top to bottom). Note the different numbers of peaks and peak halfwidths of the five diffraction patterns which indicate different degrees of structural order.

Fig. 15: Comparison of the powder XRD patterns of the layered precursor RUB-36 and the corresponding zeolite RUB-37 (zeolite framework type CDO). The shift of the first strong peak which reflects the distance between neighbouring silicate layers clearly indicates the reduction of the inter-layer distance during the condensation process from 11.1 Å to 9.2 Å.

Fig. 16: Comparison of the powder XRD patterns of the layered precursor "RUB-40, as-made" and the corresponding condensation product "RUB-40, calcined".

Fig. 17: Comparison of the solid-state ^{29}Si MAS NMR spectra of the layered precursor RUB-36 and zeolite RUB-37. Note that RUB-37 shows only one signals around -112 ppm which can be assigned to Q⁴-type silica.

Table 1: List of fer layer silicates and their condensation products published so far. Lattice parameters are: a = variable, $b \approx 14.0 \text{ \AA}$, $c \approx 7.4 \text{ \AA}$. The shift between neighbouring layers is given for an orthogonal coordination system.

As-made layer silicate			
Name, Reference	Structure directing agent (SDA)	Stacking of <u>fer</u> layers, symmetry	Synthesis Temperature [°C]
PREFER, 7	4-amino-2,2,6,6- tetramethyl-piperidine	ABAB, pseudo-orthorhombic	170
MCM-47 as made, 11	tetramethylen-bis(N- methyl)-pyrrolidinium	ABAB, orthorhombic	160
MCM-65 as made, 12,12a	quinuclidinium	ABAB, orthorhombic	160-180 preferably
PLS-1, 10	Tetramethylammonium + K ⁺	AAA, monoclinic	150
ERS-12 as made, 13	Tetramethylammonium	AAA, monoclinic	180-185
Unnamed, 14	Tetramethylammonium	No detailed structure analysis	Not given
Unnamed, 14	Diethylmethylhydroxyethylammonium	No detailed structure analysis	Not given
Unnamed, 14	Dimethylethylhydroxyethylammonium	No detailed structure analysis	Not given
Unnamed, 14	Hydroxyethyltrimethylammonium	No detailed structure analysis	Not given
Unnamed, 14	Propyltrimethylammonium	No detailed structure analysis	Not given
Unnamed, 14	N,N-Dimethylpyrrolidinium	No detailed structure analysis	Not given
Unnamed, 14	N,N-Dimethyl-3-hydroxypiperidinium	No detailed structure analysis	Not given
PLS-3, 15, 15a	Tetraethylammonium	ABAB, orthorhombic	170
PLS-4, 15a	Diethyldimethylammonium	ABAB, pseudo-orthorhombic	170
UZM-13, 16	Diethyldimethylammonium	ABAB, orthorhombic	150
UZM-17, 16	Ethyltrimethylammonium	No detailed structure analysis	150
UZM-19, 16	Diquat-4	No detailed structure analysis	165
ZSM-52, 17 ZSM-55 18	Hydroxyethyltrimethylammonium (+ Al or B)	No detailed structure analysis	

Table 2: Synthesis conditions for the preparation of layer silicates with fer layers in the system:
SiO₂ : SDAOH : H₂O.

Structure directing agent (SDA)		Molar composition of synthesis mixture			Temp. [°C]	Time [days]	Layer silicate obtained	Structure Relation, Reference
Name	C :N	SiO ₂	SDAOH	H ₂ O				
Tetramethyl-ammonium	4	1	2.8	55	160	18	RUB-20	Similar to ERS-12, 13 PLS-1, 10
Tetramethyl-phosphonium	4 (C:P)	1	1	55	160	28	RUB-40	Similar to ERS-12, 13 PLS-1, 10
Trimethyl-iso-propylammonium	6	1	0.5	20	150	15	RUB-48	Similar to UZM-13, 16 PLS-4, 15a
Diethyldimethyl-ammonium	6	1	0.5	ca. 10	150	15	RUB-36	Similar to UZM-13, 16 PLS-4, 15a
Methyltriethyl-ammonium	7	1	0.5 (SDAF)	ca. 10	150	15	RUB-38	Similar to MCM-47, 11 MCM-65, 12
								Zeolite type obtained
Dimethyldiiso-propylammonium	8	1	0.5	5 - 30	150	15	DOH, NON	
Dimethyldi-n-propylammonium	8	1	0.5	5 - 30	150	15	MFI	

Table 3: Recording conditions of the MAS and CP-MAS NMR spectra.

	¹ H ¹³ C CP-MAS	¹ H MAS	¹ H ²⁹ Si CP-MAS	²⁹ Si HPDEC MAS
Chemical shift reference	TMS	TMS	TMS	TMS
Frequency (MHz)	100.6	400.1	79.5	79.5
Pulse width (μs)	-	2 - 6.5	-	4 - 6.5
Contact time (ms)	1 - 5	-	5	-
Recycle time (s)	6	10	1	180 - 300
Spinning rate (KHz)	3.5 - 12.5	12.5	4.0	3.5 - 4.0
Number of scans	158 - 800	128 - 160	1200	229 - 1060

Table 5: Results of the ^{29}Si NMR hpdec measurements of the layered RUB materials containing fer layers. The $Q^3 : Q^4$ ratio of the interrupted layer was calculated assuming that all $\equiv\text{Si5-O12-Si5}\equiv$ groups of the idealized non-interrupted fer layer are replaced by two $\equiv\text{Si-OH}$ groups.

Material	Chemical shift [ppm]	Intensity ratio of $Q^3 : Q^4$ signals as experimentally determined by:	
		^{29}Si NMR spectroscopy	Structure analysis
Complete Layer		1 : 3.5 (idealized)	
Interrupted Layer		1 : 1.25 (idealized)	
RUB-20 (monoclinic)	Q^3 : -99.5, -103.3 (shoulder) Q^4 : -111.0, -113.7 (shoulder)	1 : 2.0	1 : 2.0
RUB-20b (monoclinic)	Q^3 : -99.5, -104.0 (shoulder) Q^4 : -111.0, -113.5 (shoulder)	1 : 2.4	1 : 2.0
RUB-40 (monoclinic)	Q^3 : -101.6, -104 (shoulder) Q^4 : -110.9, -114.1	1 : 2.3	1 : 2.2
RUB-36 (orthorhombic)	Q^3 : -104.0 Q^4 : -111.4, -114.4	1 : 3.9	1 : 3.5
RUB-38 (orthorhombic)	Q^3 : -104.3 Q^4 : -109.0, -111.0, -115.2	1 : 3.0 (CPMAS measurement)	1 : 3.5
RUB-48 (orthorhombic)	Q^3 : -103.6, -105.3 Q^4 : -109.0, -110.3, -114, -116.0	1 : 3.5	1 : 3.5

Table 6: List of signals observed from ^1H MAS NMR spectra of the layered RUB materials. The signals are assigned to certain H species. Based on the chemical shift values the corresponding O...O distances of the hydrogen bridges are calculated according to Eckert et al..³¹ The distances are compared to results of the structure analyses.

Material	Intercalated cation	Observed signals (Chemical shift [ppm])	O...O distances as calculated from the ^1H NMR chemical shift values	O...O distances between terminal oxygen atoms of neighbouring layers as obtained by the structure analysis
RUB-20	$[\text{N}(\text{CH}_3)_4]^+$	3.3 (methyl groups), 5.5 } OH groups 10.7 } involved in 13.1 } hydrogen bonding	2.87 [Å] 2.67 [Å] 2.59 [Å]	2.4(3) [Å] 2.3(3) [Å]
RUB-20b	$[\text{N}(\text{CH}_3)_4]^+$	Not determined	-	2.5(2) [Å] 2.4(3) [Å]
RUB-40	$[\text{P}(\text{CH}_3)_4]^+$	2.1 (methyl groups), 5.5 } OH groups 10.7 } involved in 13.0 } hydrogen bonding	2.87 [Å] 2.67 [Å] 2.59 [Å]	2.55(3) [Å] 2.31(4) [Å]
RUB-36	$[\text{N}(\text{CH}_3)_2(\text{CH}_2\text{CH}_3)_2]^+$	1.5 (methyl groups attached to carbon), 3.5 (methyl and methylene groups attached to N) 16.5 (Hydrogen bridge)	2.45 [Å]	2.35(4) [Å]
RUB-38	$[\text{N}(\text{CH}_3)_1(\text{CH}_2\text{CH}_3)_3]^+$	1.5 (methyl groups attached to carbon), 3.5 (methyl and methylene groups attached to N) 17 (Hydrogen bridge)	2.40 [Å]	2.37(6) [Å]
RUB-48	$[\text{N}(\text{CH}_3)_3\{\text{CH}(\text{CH}_3)_2\}_1]^+$	1.5 (methyl groups attached to carbon), 3.5 (methyl and methylene groups attached to N) 16.6 (Hydrogen bridge)	2.45 [Å]	2.41(11) [Å]

Table 7: Results of the thermal analysis (TG and DTA).

Sample	Composition (according to Rietveld refinement and NMR spectra)	Endo- thermic signal [°C]	Exo- thermic signal(s) [°C]	Calculated amount of SDA and Water [%]	Total weight loss [%]
RUB-20	$\text{Si}_{18}\text{O}_{35}(\text{OH})_4 [\text{N}(\text{CH}_3)_4]_{1.7}$	343	455	15.6	16.6
RUB-20b	$\text{Si}_{18}\text{O}_{35}(\text{OH})_4 [\text{N}(\text{CH}_3)_4]_{1.9}$	330+403	448	15.6	15.8
RUB-40	$\text{Si}_{18}\text{O}_{35.2}(\text{OH})_{3.6} [\text{P}(\text{CH}_3)_4]_{1.8}$	321	548	17.4	6.5 *
RUB-36	$\text{Si}_{36}\text{O}_{72}(\text{OH})_4 [\text{N}(\text{CH}_3)_2(\text{CH}_2\text{CH}_3)_2]_4$	373	415 + 439	18.2	18.2
RUB-38	$\text{Si}_{36}\text{O}_{72}(\text{OH})_4 [\text{N}(\text{CH}_3)_1(\text{CH}_2\text{CH}_3)_3]_4$	322	357 + 373	19.9	19.4
RUB-48	$\text{Si}_{36}\text{O}_{72}(\text{OH})_4 [\text{N}(\text{CH}_3)_3\{\text{CH}(\text{CH}_3)_2\}_1]_4$	353	430	18.2	18.6

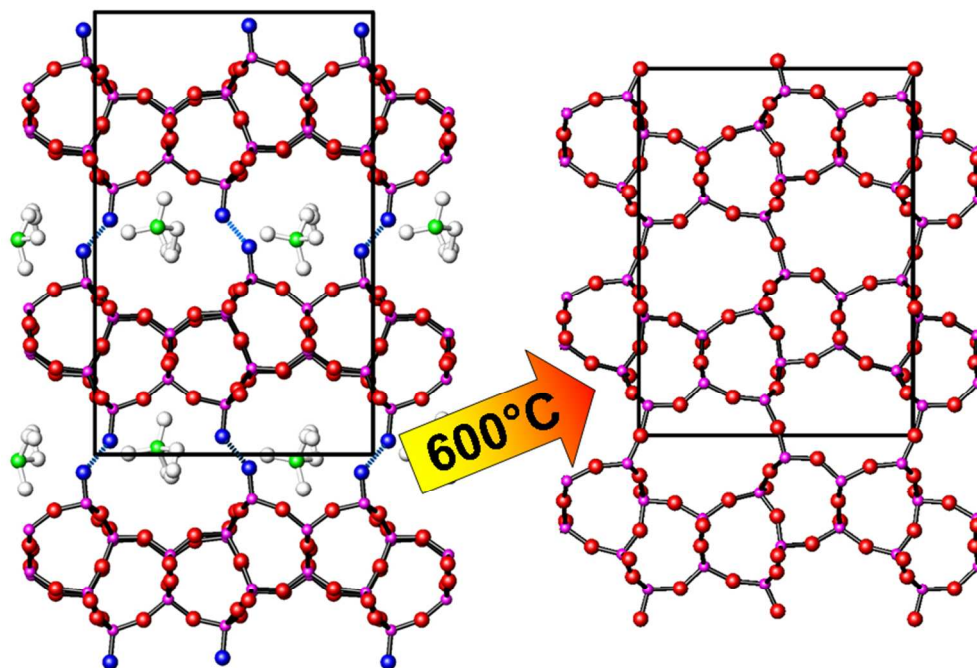
* the sample is gray after the heating indicating that a part of the organic material could not be removed. The $\text{P}(\text{CH}_3)_4^+$ was probably oxidized to a phosphate. All other samples are colourless.

Table 8: List of HLSs and corresponding framework silicates containing fer layers. d_{L-L} = distance between neighbouring layers. Shift vector = Shift vector between neighbouring layers

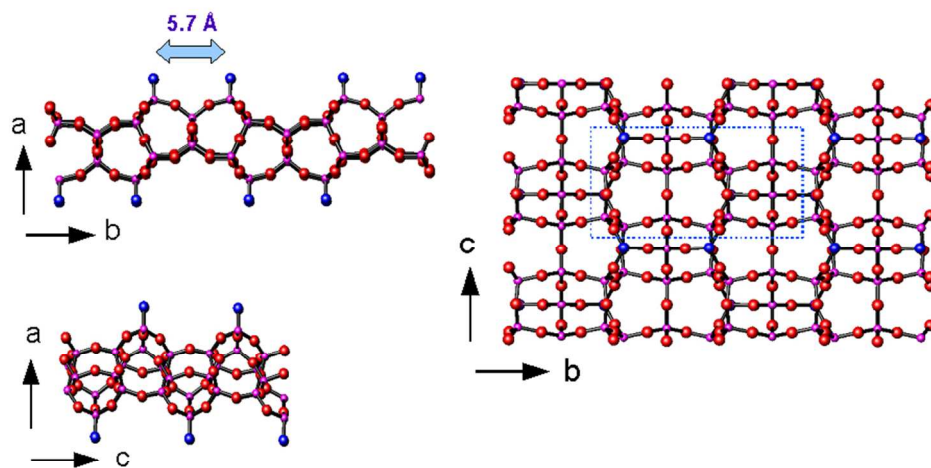
As-made Hydrous Layer Silicate					Framework silicate	
Name	Cation	Layer arrangement, Shift vector	Symmetry	d_{L-L}	Name	Zeolite Framework Type, degree of order
RUB-20	Tetramethylammonium	MONO-1, AAA-stacking, $0 b_0 + 0.19 c_0$	$P2_1/m$	10.4	RUB-20 calcined	-, highly disordered
RUB-40	Tetramethylphosphonium	MONO-1, AAA-stacking, $0 b_0 + 0.24 c_0$	$P2_1/m$	10.6	RUB-40 calcined	CDO, poorly ordered
PLS-1	Tetramethylammonium + K^+	MONO-1, AAA-stacking, $0 b_0 + 0.20 c_0$	$P2_1/m$	10.5	CDS-1	CDO, poorly ordered
ERS-12	Tetramethylammonium	MONO-1, AAA-stacking, $0 b_0 + 0.20 c_0$	$P2_1$	10.6	ERS-12 calcined	-, highly disordered
RUB-36	Diethyl-dimethylammonium	ORTHO-3, ABAB-stacking, $0 b_0 \pm 0.36 c_0$	$Pn2_1a$	11.1	RUB-37	CDO, well ordered
PLS-4	Diethyl-dimethylammonium	ORTHO-3, ABAB-stacking, $0 b_0 \pm 0.32 c_0$	$P2_1/c$ ($\beta = 89.8^\circ$)	11.1	CDO-type	CDO, well ordered
UZM-13	Diethyl-dimethylammonium	ORTHO-3, ABAB-stacking, $0 b_0 \pm 0.38 c_0$	$Pnma$	11.1	UZM-25	CDO, well ordered
RUB-48	Trimethylisopropylammonium	ORTHO-3, ABAB-stacking, $0 b_0 \pm 0.39 c_0$	$Pn2_1a$	11.1	RUB-49	CDO, fairly ordered
RUB-38	Methyltriethylammonium	ORTHO-2, ABAB-stacking, $0 b_0 + 1/2 c_0$	$Bbmm$	11.3	RUB-37	CDO, fairly ordered
MCM-47	Tetramethylen-bis(N-methylpyrrolidinium)	ORTHO-2, ABAB-stacking, $0 b_0 + 1/2 c_0$	$Bbmm$	11.2	MCM-47 calcined	-, highly disordered
MCM-65	Quinuclidinium + Tetramethylammonium	ORTHO-2, ABAB-stacking, $0 b_0 + 1/2 c_0$	o'rhomb	11.3	MCM-65 calcined	CDO, fairly ordered
PREFER	4-amino-2,2,6,6-tetramethylpiperidine	ORTHO-1, ABAB-stacking, $1/2 b_0 + 1/2 c_0$	pseudo o'rhomb	13.7	Silica Ferrierite	FER well ordered
PLS-3	Tetraethylammonium	ORTHO-1, ABAB-stacking $1/2 b_0 + 1/2 c_0$		11.7	CDS-3	FER, well ordered

Table 4: Experimental and crystallographic parameters for the structure refinements of the silicates analyzed. d_{L-L} = distance between neighbouring layers. The nearly identical structures of RUB-20 and RUB-20b can as well be described based on space group symmetry $P2_1$. RUB-20b contained a small amount of Nonasil which was included in the refinement.

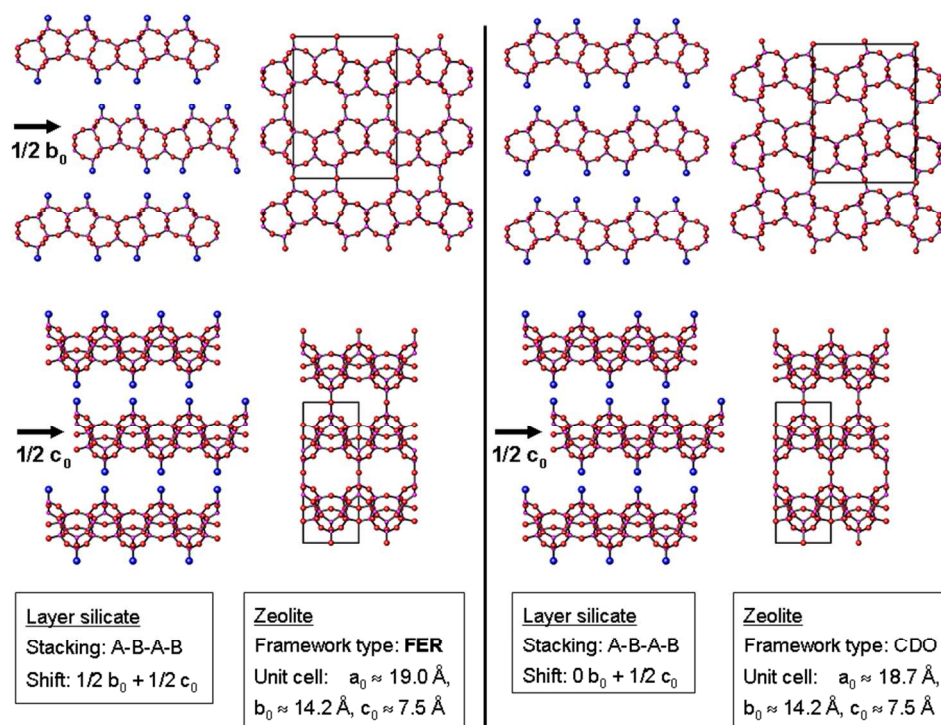
	RUB-36	RUB-38	RUB-48	RUB-20	RUB-20b	RUB-40	RUB-37
Diffractometer	Synchrotron						
	$\lambda = 1.131406 \text{ \AA}$						
2θ range of data [$^\circ$]	5.5 - 50.0	7.0 - 80.0	7.0 - 85.0	7.0 - 83.5	7.0 - 83.5	7.5 - 83.5	9.0 - 80.0
Step size [$^\circ 2\theta$]	0.003	0.0078	0.0078	0.0078	0.0078	0.0078	0.0078
No. steps	14828	9359	10000	9808	9757	9744	9103
No. contr. reflections	562	686	998	923	910	1023	558
No. geometric restraints	122	45	124	79	79	79	63
No. structural parameters	109	37	110	64	64	64	48
No. profile parameters	19	18	17	21	21	22	18
R_{Bragg}	0.065	0.055	0.048	0.033	0.032	0.051	0.065
R_{wp}	0.179	0.184	0.147	0.080	0.078	0.144	0.163
R_{exp}	0.108	0.162	0.080	0.046	0.039	0.104	0.128
χ^2	2.7	1.3	3.5	3.1	3.9	1.9	1.6
Space group	$Pn2_1a$ (No. 33)	$Bbmm$ (No.63)	$Pn2_1a$ (No. 33)	$P2_1/m$ (No. 11)	$P2_1/m$ (No. 11)	$P2_1/m$ (No. 11)	$Bb21m$ (No. 36)
a_0 [\AA]	22.239(2)	22.559 (3)	22.281 (2)	10.493 (2)	10.628 (2)	10.764(2)	18.412(2)
b_0 [\AA]	14.025(2)	13.993(2)	14.000(2)	13.988(2)	13.965(2)	14.001(2)	13.791(2)
c_0 [\AA]	7.391(1)	7.369(1)	7.383(1)	7.411(1)	7.411(1)	7.407(1)	7.383(1)
β [$^\circ$]	90	90	90	97.80	98.29	99.34	90
d_{L-L} [\AA]	11.1	11.3	11.1	10.4	10.5	10.6	9.2
Unit cell content	$[\text{Si}_{36}\text{O}_{72}(\text{OH})_4]$	$[\text{Si}_{36}\text{O}_{72}(\text{OH})_4]$	$[\text{Si}_{36}\text{O}_{72}(\text{OH})_4]$	$[\text{Si}_{18}\text{O}_{35}(\text{OH})_4]$	$[\text{Si}_{18}\text{O}_{35}(\text{OH})_4]$	$[\text{Si}_{16}\text{O}_{35.2}(\text{OH})_{3.6}]$	$[\text{Si}_{16}\text{O}_{72}]$
	* 4 $\text{C}_6\text{H}_{16}\text{N}$	* 4 $\text{C}_7\text{H}_{18}\text{N}$	* 4 $\text{C}_6\text{H}_{16}\text{N}$	* 1.7 $\text{C}_4\text{H}_{12}\text{N}$	* 1.9 $\text{C}_4\text{H}_{12}\text{N}$	* 1.8 $\text{C}_4\text{H}_{12}\text{P}$	



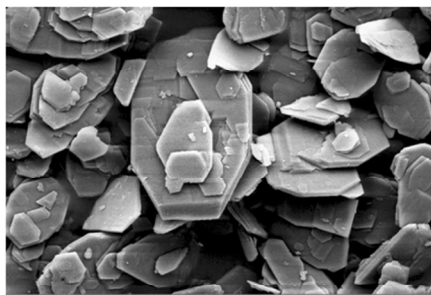
Hydrous Layered Silicates containing Ferrihydrite-type layers are a structurally versatile family of materials which can be converted into microporous silicates by topotactic condensation or interlayer expansion.



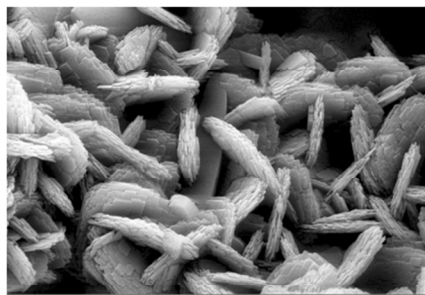
254x190mm (96 x 96 DPI)



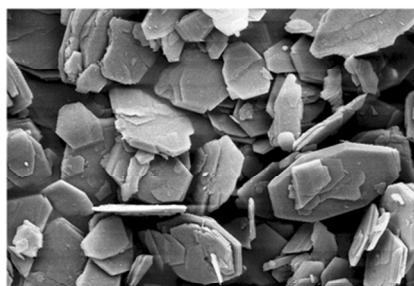
254x190mm (96 x 96 DPI)



10 μm

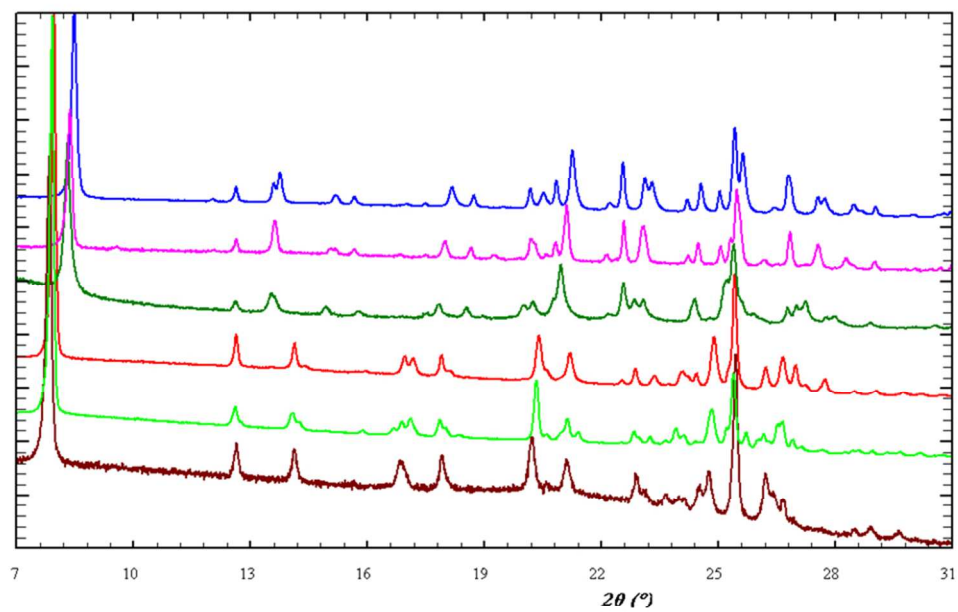


2 μm

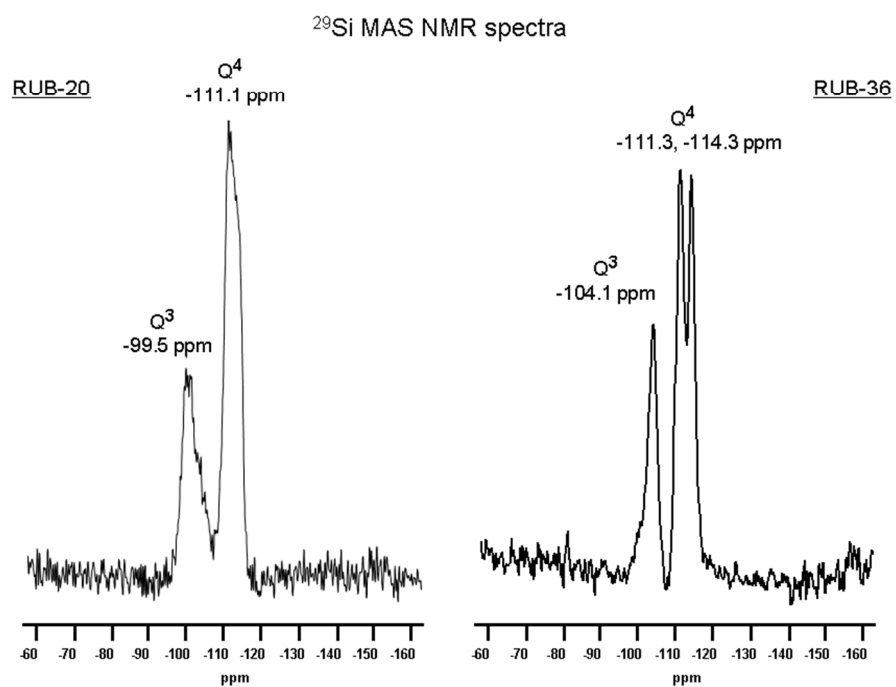


10 μm

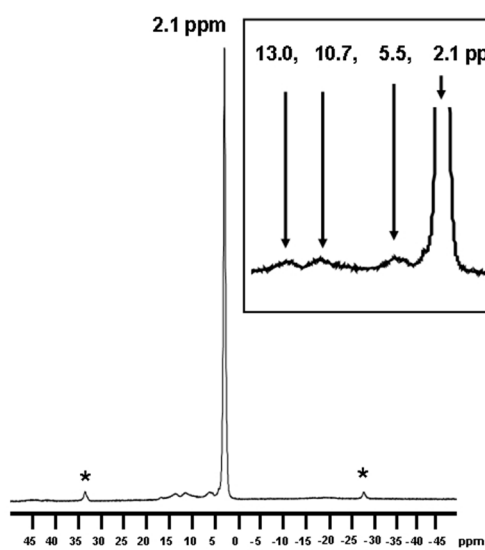
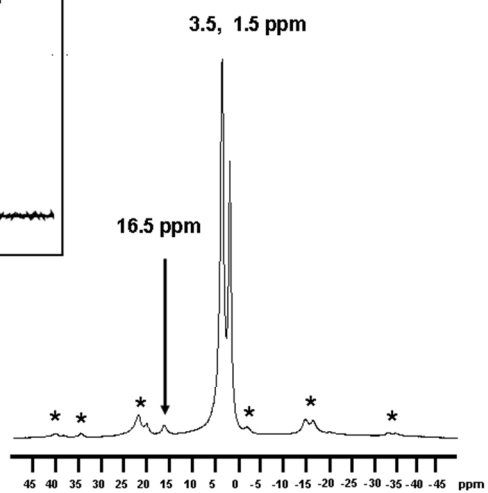
254x190mm (96 x 96 DPI)



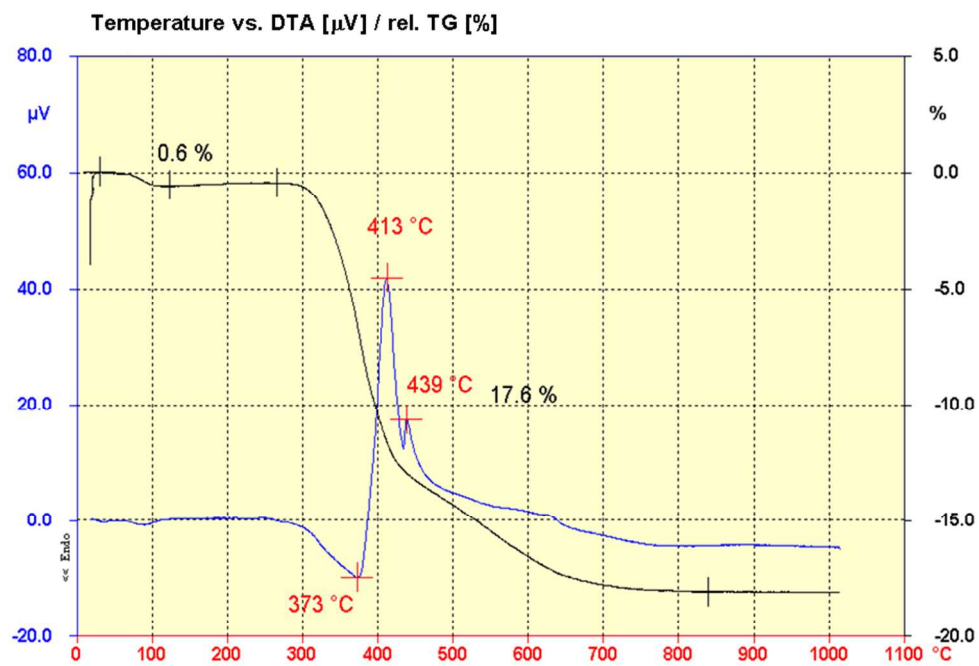
254x190mm (96 x 96 DPI)



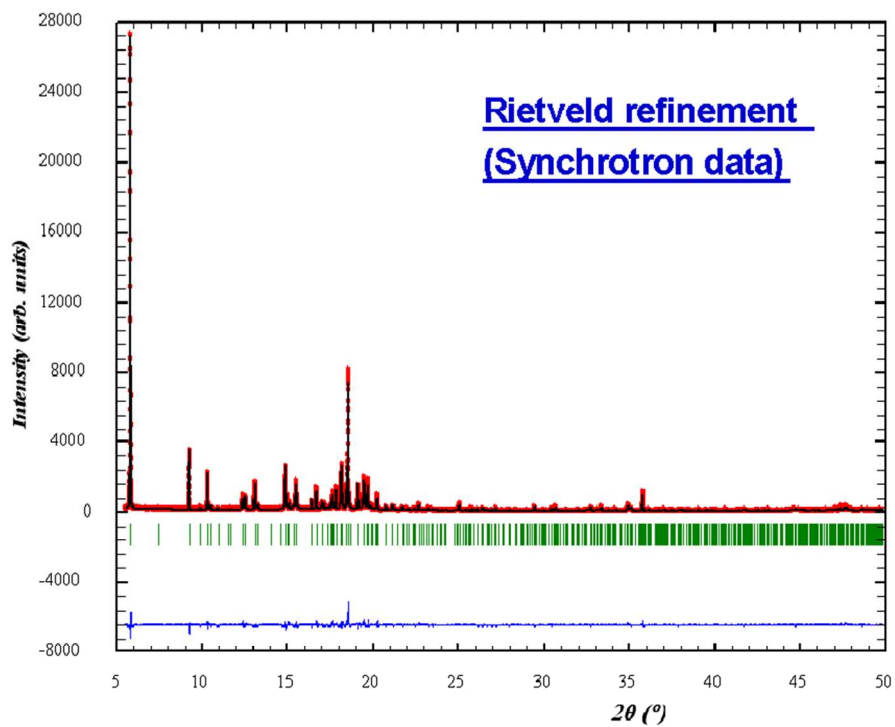
254x190mm (96 x 96 DPI)

^1H MAS NMR of RUB-20 ^1H MAS NMR of RUB-36

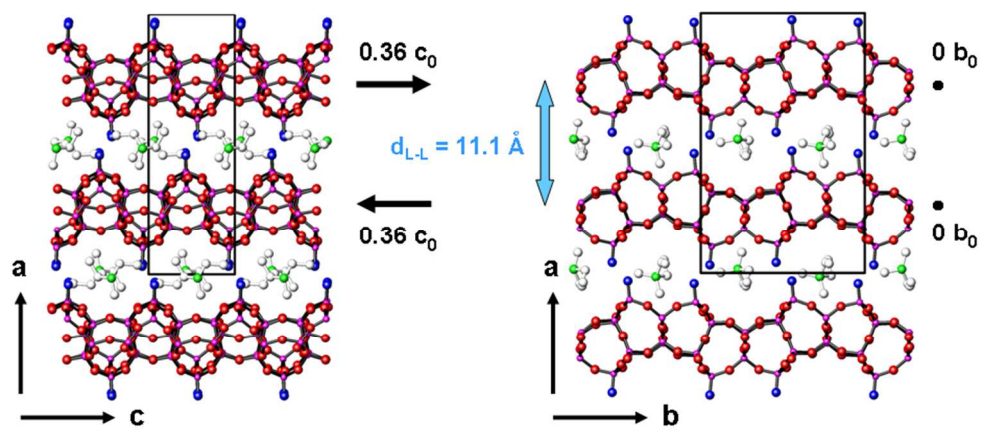
254x190mm (96 x 96 DPI)



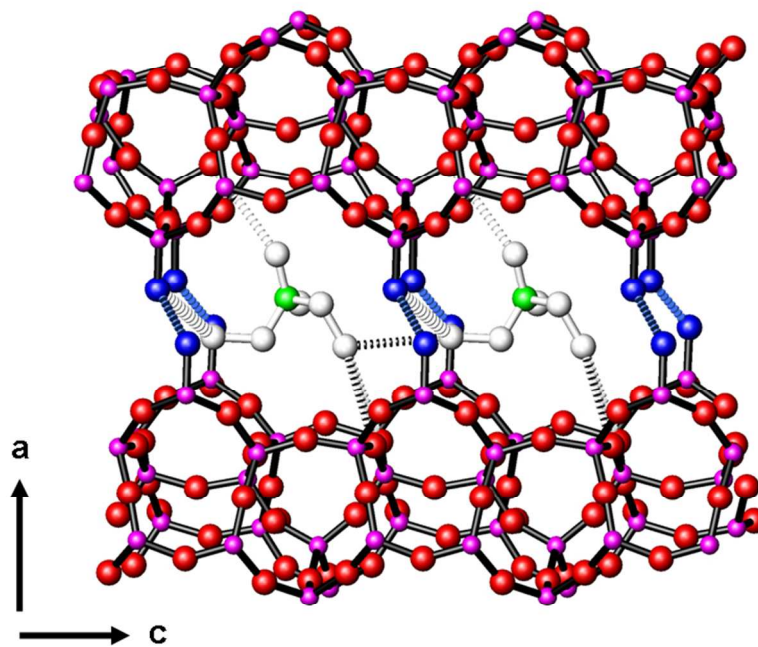
254x190mm (96 x 96 DPI)



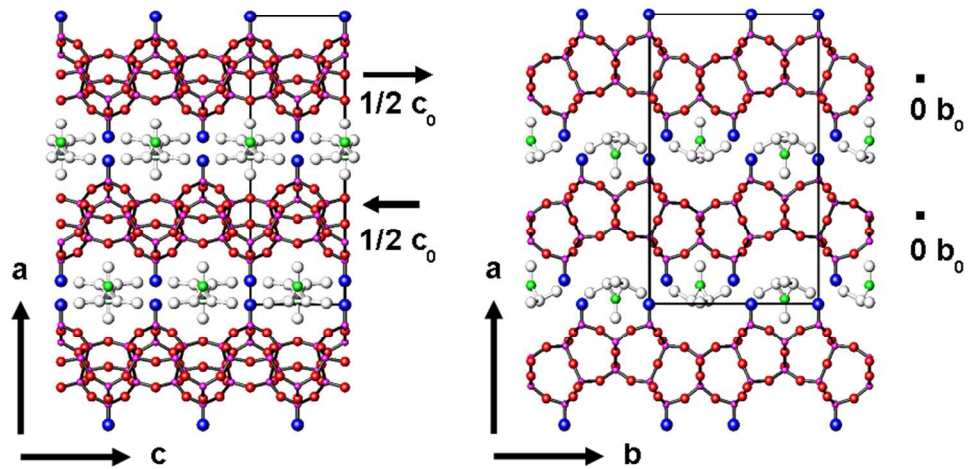
254x190mm (96 x 96 DPI)



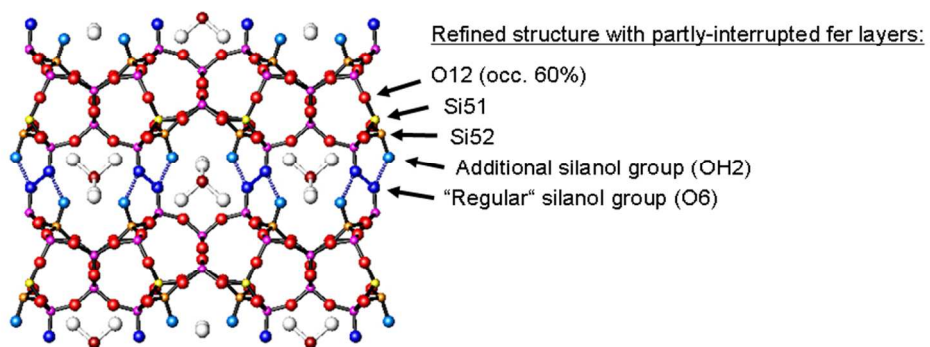
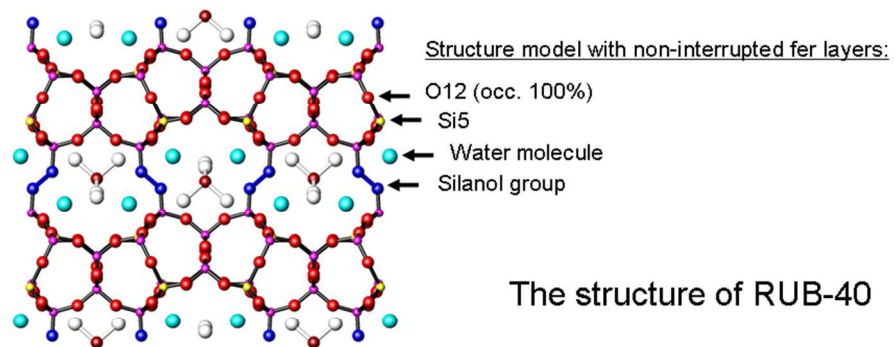
254x190mm (96 x 96 DPI)



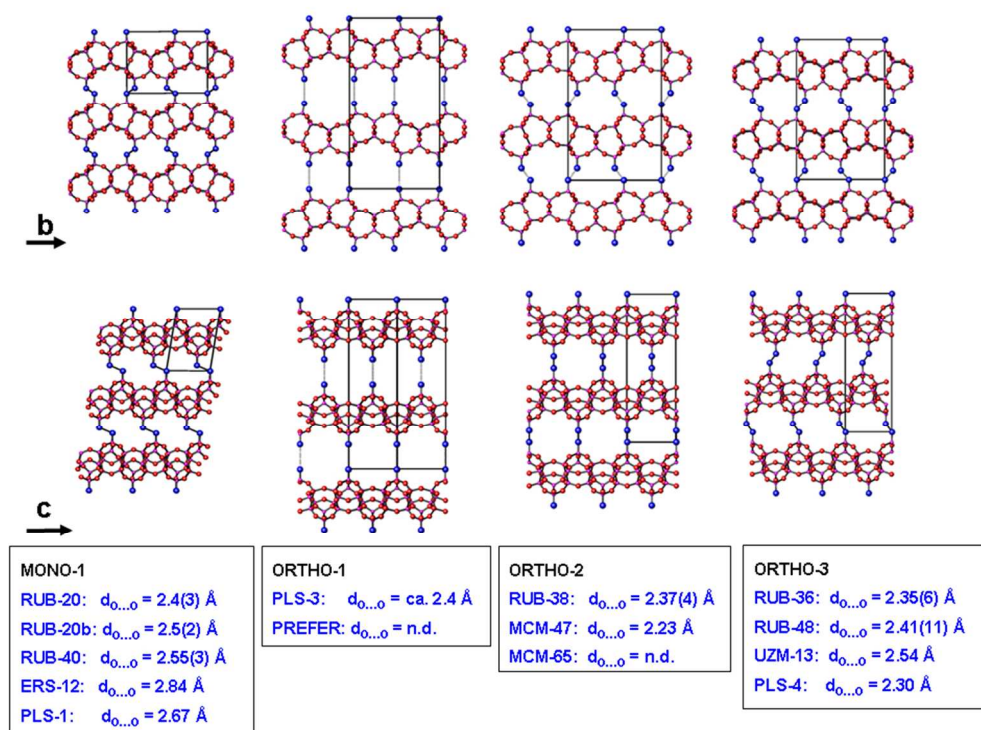
254x190mm (96 x 96 DPI)



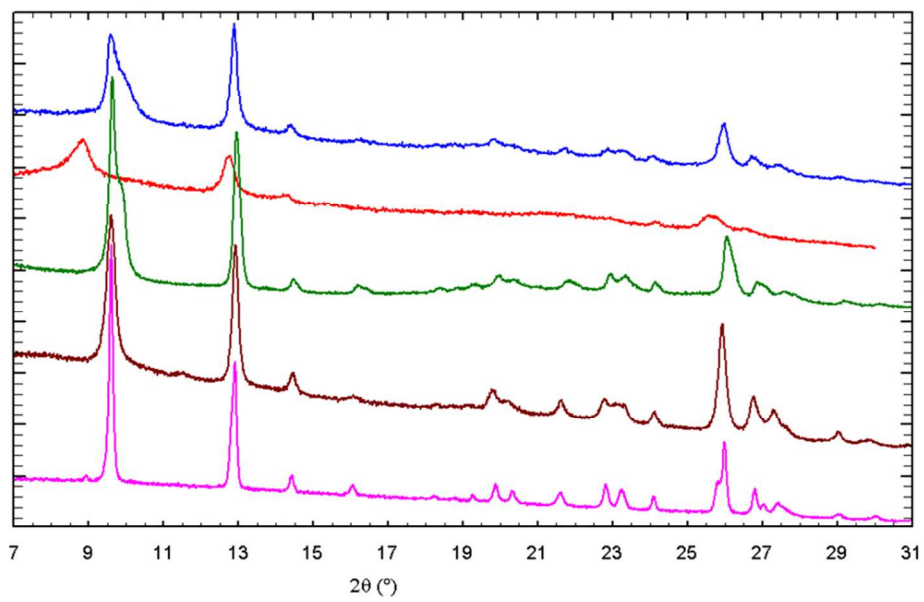
254x190mm (96 x 96 DPI)



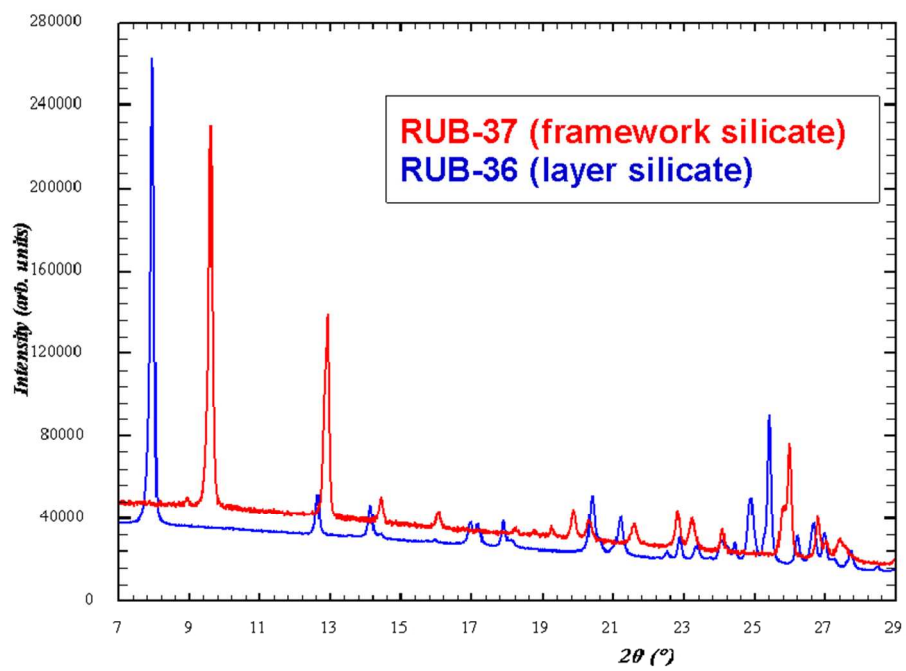
254x190mm (96 x 96 DPI)



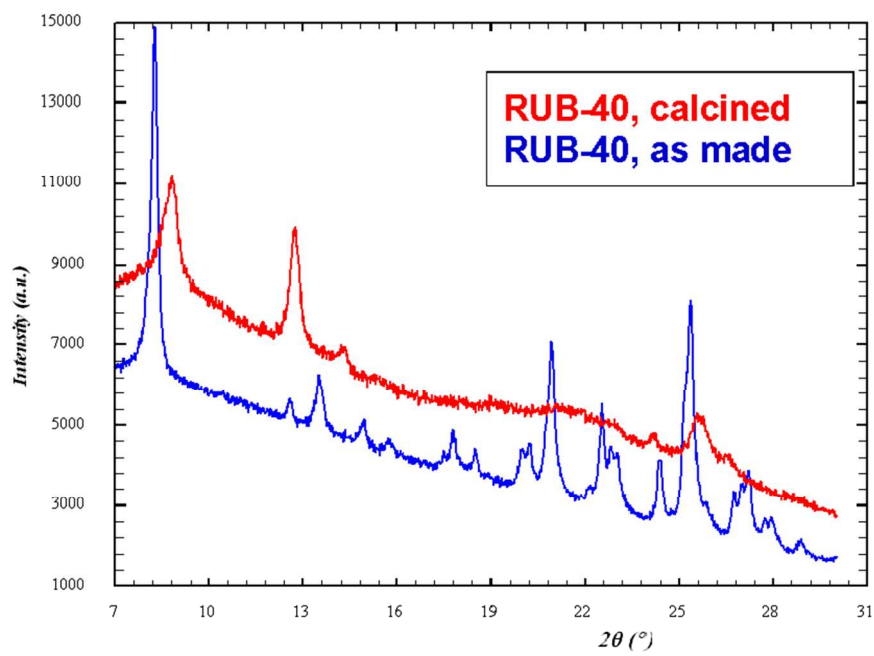
254x190mm (96 x 96 DPI)



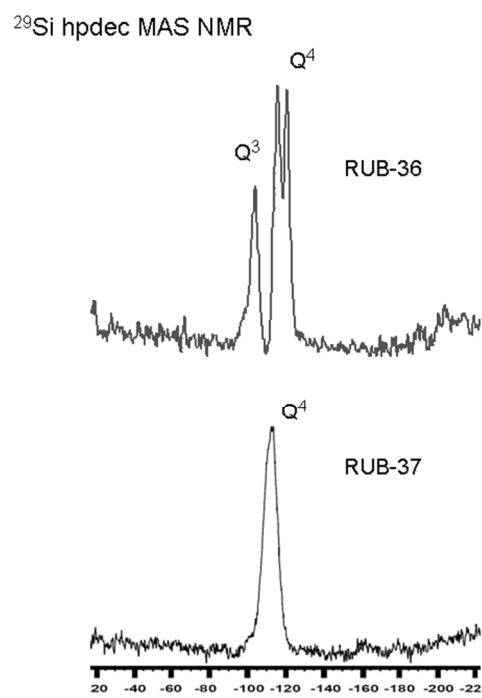
254x190mm (96 x 96 DPI)



254x190mm (96 x 96 DPI)



254x190mm (96 x 96 DPI)



254x190mm (96 x 96 DPI)